RESEARCH ARTICLE

Epigenetic Activation of Plasmacytoid DCs Drives IFNAR-Dependent Therapeutic Differentiation of AML

Jessica M. Salmon[1,2], Izabela Todorovski[1,3], Kym L. Stanley[1], Claudia Bruedigam[4,5], Conor J. Kearney[1,3], Luciano G. Martelotto[6], Fernando Rossello[6,7], Timothy Semple[8], Gisela Mir Arnau[3,8], Magnus Zethoven[1], Michael Bots[9], Stefan Bjelosevic[1,3], Leonie A. Cluse[1], Peter J. Fraser[1], Veronique Litalien[2], Eva Vidacs[1], Kate McArthur[10], Antony Y. Matthews[11], Elise Gressier[12], Nicole A. de Weerd[11], Jens Lichte[13], Madison J. Kelly[1], Simon J. Hogg[1,3], Paul J. Hertzog[11], Lev M. Kats[1,3], Stephin J. Vervoort[1,3], Daniel D. De Carvalho[14], Stefanie Scheu[13], Sammy Bedoui[12], Benjamin T. Kile[10,15], Steven W. Lane[4,5], Andrew C. Perkins[2], Andrew H. Wei[2], Pilar M. Dominguez[1,3], and Ricky W. Johnstone[1,3]

Illustration by Bianca Dunn

ABSTRACT Pharmacologic inhibition of epigenetic enzymes can have therapeutic benefit against hematologic malignancies. In addition to affecting tumor cell growth and proliferation, these epigenetic agents may induce antitumor immunity. Here, we discovered a novel immunoregulatory mechanism through inhibition of histone deacetylases (HDAC). In models of acute myeloid leukemia (AML), leukemia cell differentiation and therapeutic benefit mediated by the HDAC inhibitor (HDACi) panobinostat required activation of the type I interferon (IFN) pathway. Plasmacytoid dendritic cells (pDC) produced type I IFN after panobinostat treatment, through transcriptional activation of IFN genes concomitant with increased H3K27 acetylation at these loci. Depletion of pDCs abrogated panobinostat-mediated induction of type I IFN signaling in leukemia cells and impaired therapeutic efficacy, whereas combined treatment with panobinostat and IFNα improved outcomes in preclinical models. These discoveries offer a new therapeutic approach for AML and demonstrate that epigenetic rewiring of pDCs enhances antitumor immunity, opening the possibility of exploiting this approach for immunotherapies.

SIGNIFICANCE: We demonstrate that HDACis induce terminal differentiation of AML through epigenetic remodeling of pDCs, resulting in production of type I IFN that is important for the therapeutic effects of HDACis. The study demonstrates the important functional interplay between the immune system and leukemias in response to HDAC inhibition.

INTRODUCTION

Two of the most prevalent cytogenetic subtypes of primary acute myeloid leukemia (AML), t(8;21) and inv(16), involve genes encoding the core binding factors (CBF) AML1 and CBFβ, respectively (1). Although CBF-associated AML is considered "favorable risk," close to 50% of patients will relapse at 5 years and die of their disease (2). The t(8;21) translocation produces the AML1–RUNX1T1 fusion oncoprotein (also called AML1–ETO), which affects the normal transcriptional activity of AML1 (3, 4). In addition, mutations in NRAS/KRAS frequently co-occur in patients with t(8;21) AML (5). We previously established a mouse model with pathologic and molecular features of human AML, initiated by the constitutive coexpression of AML1–ETO9a (containing a transcript with alternative splicing in exon 9 of *ETO*) and an oncogenic allele of NRAS ($NRAS^{G12D}$) in mouse hemopoietic progenitor cells (6, 7). We and others previously showed that AML1–ETO can recruit histone deacetylases (HDAC; refs. 7–9), resulting in repression of AML1-target genes and suppression of hemopoietic cell differentiation to promote leukemogenesis. Importantly, treatment with HDAC inhibitors (HDACi) induced terminal differentiation of leukemia cells and enhanced survival in t(8;21) AML mouse models (7). Mixed lineage leukemia (MLL) rearrangements are also frequent in leukemias and are considered an adverse risk factor. MLL fusion proteins can form complexes with various transcriptional, epigenetic, and structural proteins including positive transcription elongation factor B (pTEFB), HDACs, and the tumor suppressor Menin (10), and coinhibition of HDAC and MLL–menin interaction induces apoptosis of leukemia cells (11).

[1]Translational Haematology Program, Peter MacCallum Cancer Centre, Melbourne, Victoria, Australia. [2]Australian Centre for Blood Diseases, Monash University and The Alfred Hospital, Melbourne, Australia. [3]The Sir Peter MacCallum Department of Oncology, University of Melbourne, Parkville, Victoria, Australia. [4]Cancer Program, Queensland Institute of Medical Research (QIMR) Berghofer Medical Research Institute, Brisbane, Queensland, Australia. [5]School of Medicine, University of Queensland, Brisbane, Queensland, Australia. [6]Single Cell Innovation Lab, Department of Clinical Pathology, University of Melbourne, Parkville, Victoria, Australia. [7]University of Melbourne Centre for Cancer Research, The University of Melbourne, Melbourne, Victoria, Australia. [8]Molecular Genomics Core, Peter MacCallum Cancer Centre, Melbourne, Victoria, Australia. [9]Laboratory of Clinical Chemistry, Academic Medical Center, University of Amsterdam, the Netherlands. [10]Anatomy and Developmental Biology, Monash Biomedicine Discovery Institute, Monash University, Melbourne, Victoria, Australia. [11]Centre for Innate Immunity and Infectious Diseases, Hudson Institute of Medical Research, Clayton, Victoria, Australia; Department of Molecular and Translational Sciences, Monash University Clayton Victoria, Australia. [12]Department of Microbiology and Immunology at the Peter Doherty Institute for Infection and Immunity, University of Melbourne, Parkville, Victoria, Australia. [13]Institute of Medical Microbiology and Hospital Hygiene, University of Düsseldorf, Düsseldorf, Germany. [14]Princess Margaret Cancer Centre, University Health Network, Toronto, Canada; Department of Medical Biophysics, University of Toronto, Toronto, Canada. [15]Faculty of Health and Medical Sciences, University of Adelaide, Adelaide, South Australia, Australia.

Note: Supplementary data for this article are available at Cancer Discovery Online (http://cancerdiscovery.aacrjournals.org/).

J.M. Salmon and I. Todorovski contributed equally to this article.

P.M. Dominguez and R.W. Johnstone are co–senior authors.

Corresponding Authors: Ricky W. Johnstone, Peter MacCallum Cancer Centre, 305 Grattan Street, Melbourne, Victoria 3000, Australia. Phone: 61-855-97133; E-mail: ricky.johnstone@petermac.org; and Pilar M. Dominguez, Peter MacCallum Cancer Centre, 305 Grattan Street, Melbourne, Victoria 3000, Australia. Phone: 61-481-880-373; E-mail: pilar.dominguez@petermac.org

Cancer Discov 2022;12:1560–79

doi: 10.1158/2159-8290.CD-20-1145

Although a number of HDACis have been approved by the FDA for hematologic malignancies (12), their therapeutic impact as single agents has been modest. Studies using genetically and histologically distinct preclinical cancer models demonstrated that the efficacy of HDACis was reduced in immune-compromised recipient mice or following immune cell depletion in wild-type mice, indicating an immune-dependent component in their mechanism of action (13). In line with this, recent studies have shown promising results of combining HDACis with immunotherapy (14). Although these reports point to the ability of HDACis to engage the host immune system, exactly how this is achieved remains ill-defined. Previous studies have focused on the ability of HDACis to enhance the immunogenicity of tumor target cells by promoting the expression of key immune-modulating genes that are epigenetically silenced during tumor immune evasion (15, 16). However, the impact of these agents on the activity of other cells in the tumor microenvironment, in particular cells that regulate host and/or tumor immunity, has been less well studied.

Here we investigated the genes and molecular pathways altered by HDACis in different models of AML. Our results reveal that the HDACi panobinostat induced plasmacytoid dendritic cells (pDC) to increase expression of type I interferon (IFN). The combined effect of panobinostat and pDC-derived IFN resulted in leukemia cell differentiation *in vivo* and a pronounced therapeutic outcome. Perturbation of this combined effect through genetic deletion of the type I IFN receptor (IFNAR) on the leukemia cells or depletion of pDCs *in vivo* significantly abrogated the therapeutic effects of panobinostat. Moreover, the combinatorial effects of panobinostat and type I IFN could be therapeutically exploited through the addition of recombinant IFNα to the panobinostat therapy regimen that resulted in greatly enhanced therapeutic benefit. This is the first study demonstrating that HDACis can mediate profound antitumor responses through immune-modulatory effects on pDCs resulting in enhanced type I IFN gene transcription. The resultant type I IFN is necessary for HDACi-induced leukemia differentiation and therapeutic benefit, identifying a unique molecular interplay between effects of epigenetic agents on the tumor target cells and host immune cells.

RESULTS

Panobinostat Induces Differentiation of AML Cells through Activation of the Type I Interferon Pathway

A preclinical mouse model of t(8;21) AML developed through retroviral expression of AML1–ETO9a and NRAS^{G12D} (A/E9a;NRAS^{G12D}) in hematopoietic cells (6, 7) was utilized to study the therapeutic effects of HDACis and decipher the molecular events that underpinned their anticancer activities (Supplementary Fig. S1A). Treatment of mice bearing A/E9a;NRAS^{G12D} AML with panobinostat resulted in reduced tumor burden compared with vehicle-treated animals as assessed by reduced GFP$^+$ cells in the peripheral blood (Fig. 1A) and a decrease in bioluminescence (Fig. 1B). The panobinostat-induced reduction in leukemia cell numbers manifested in a significant median survival advantage of 38.5 days (Fig. 1C). We previously showed that treatment of A/E9a;NRAS^{G12D} leukemias with panobinostat resulted in leukemia cell-cycle arrest and myeloid differentiation (7, 17). To determine the minimum panobinostat treatment time required for t(8;21) AML cells to undergo differentiation, leukemia cells were harvested from the bone marrow over the first week of therapy for assessment. BrdU incorporation assays demonstrated that panobinostat reduced leukemia cell proliferation from day 3 onward, with only approximately 10% of cells in the panobinostat cohort in S-phase after 5 days of therapy compared with 40% of cells in S-phase in the vehicle-treated group (Fig. 1D). Consistent with our previous studies (6, 7), panobinostat treatment resulted in decreased expression of c-Kit and increased expression of CD11b (Fig. 1E), indicating terminal myeloid differentiation toward the granulocyte lineage. Treatment with panobinostat of two MLL-driven leukemias—MLL/ENL (M/E;NRAS^{G12D}) and MLL/AF9 (M/A;NRAS^{G12D})—also induced leukemia cell differentiation with significant increased levels of Sca-1, reduced expression of c-Kit, and a trend toward increased CD11b expression (Supplementary Fig. S1B and S1C).

To determine the transcriptional changes that might underpin the induction of differentiation of leukemia cells following exposure to panobinostat, RNA sequencing (RNA-seq) was performed on leukemias harvested from tumor-bearing mice treated with either vehicle or panobinostat for 3 days, the point at which panobinostat-treated AML cells are demonstrating features of differentiation. Principal component analysis (PCA) showed a clear separation between the transcriptional profiles of leukemia cells from panobinostat-treated or vehicle-treated (control) mice (Supplementary Fig. S1D). A supervised analysis identified 669 differentially expressed genes (DEG) in leukemias harvested from panobinostat-treated and control mice [log fold change (logFC) > 1, $P_{adj} < 0.05$], the majority of which were upregulated after panobinostat treatment ($n = 397$; Fig. 1F; Supplementary Table S1). Pathway analysis of these upregulated genes through gene set enrichment analysis (GSEA) and gene ontology (GO) enrichment revealed significant enrichment of genes associated with type I IFN and antiviral responses, as well as IFN gamma (IFNγ) response, p53 pathway and cytokine signaling, including IL6 and TNFα (Fig. 1F and G; Supplementary Fig. S1E). Upregulation of transcription factors primarily involved in type I IFN signaling (*Stat1*, *Stat2*, *Irf1*, and *Irf9*) was prevalent, and a concomitant increase in expression of STAT target genes *Mx2* and *2′5′Oas* was observed (Fig. 1F and H; Supplementary Table S1). qRT-PCR was used as an orthogonal method to confirm the increased expression of *Stat1*, *Stat2*, and *Oas2* in leukemia cells exposed to panobinostat for 3 days *in vivo* (Fig. 1I).

Expression of IFNAR1 on A/E9a;NRAS^{G12D} Leukemia Cells Is Critical for the Efficacy of Panobinostat *In Vivo*

Type I IFN signaling through IFNAR expressed on tumor cells can induce cell-cycle arrest and cell death (18, 19). We analyzed IFNAR expression on the surface of leukemia cells in panobinostat-treated mice compared with vehicle-treated or untreated mice and found no difference (Supplementary Fig. S2A). To determine the functional and therapeutic

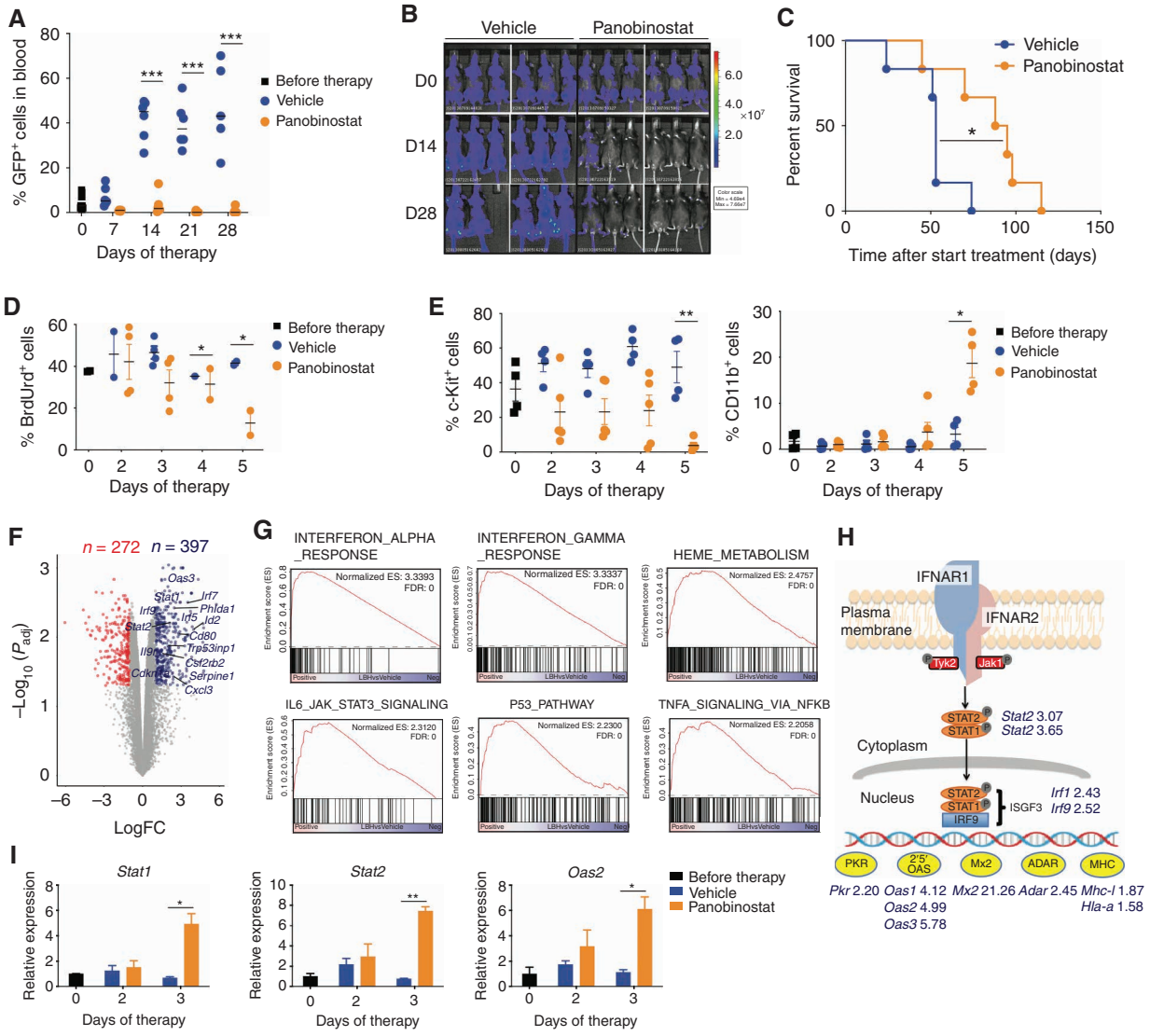

Figure 1. Panobinostat induces differentiation of AML cells through activation of the type I interferon pathway. **A,** Percentage of GFP-positive cells in the peripheral blood of mice bearing A/E9a;NRAS^{G12D}-driven leukemias treated with vehicle or panobinostat ($n = 5$–6 mice/group; ***, $P < 0.001$). **B,** Bioluminescence imaging of individual tumor-bearing animals over the course of therapy with vehicle or panobinostat. **C,** Kaplan–Meier survival curves of mice bearing A/E9a;NRAS^{G12D}-driven leukemias treated with vehicle or panobinostat ($n = 6$ mice/group; *, $P < 0.05$). **D,** Cell-cycle analysis of A/E9a;NRAS^{G12D} leukemia cells within the bone marrow of animals treated with vehicle or panobinostat. The percentage of cells in S-phase (BrdU-positive) was determined by flow cytometry ($n = 3$; *, $P < 0.05$). **E,** Flow-cytometric analysis of the cell-surface expression of c-Kit and CD11b on tumor cells in the bone marrow of A/E9a;NRAS^{G12D} tumor–bearing mice treated for 5 days with vehicle or panobinostat ($n = 3$; *, $P < 0.05$; **, $P < 0.005$). **F,** Volcano plot of the DEG (logFC > 1; $P_{adj} < 0.05$) between A/E9a;NRAS^{G12D} cells isolated from panobinostat-treated and vehicle-treated leukemia-bearing mice. **G,** GSEA of upregulated genes shown in **F**. **H,** IFNAR signaling pathway and increased fold change in individual genes induced by panobinostat treatment. **I,** Expression by qRT-PCR of *Stat1*, *Stat2*, and *2′5′Oas* on tumor cells isolated from vehicle- and panobinostat-treated animals over 3 days of therapy ($n = 3$; *, $P < 0.05$; **, $P < 0.005$).

relevance of type I IFN signal activation following exposure of A/E9a;NRAS^{G12D} AML to panobinostat, leukemias with genetic knockout of *Ifnar1* were developed by transducing fetal liver cells harvested from *Ifnar1*$^{-/-}$ mice (20) with retroviral constructs expressing AML1–ETO9a and NRAS^{G12D} (Fig. 2A). Strikingly, when wild-type mice transplanted with A/E9a;NRAS^{G12D};*Ifnar1*$^{-/-}$ leukemias were treated with panobinostat, the therapeutic benefit of panobinostat observed in mice bearing A/E9a;NRAS^{G12D} AML was lost (Fig. 2B). This result was further confirmed in two additional independently derived A/E9a;NRAS^{G12D};*Ifnar1*$^{-/-}$ leukemias (Supplementary Fig. S2B). A readout for panobinostat activity in A/E9a;NRAS^{G12D} leukemias is degradation of the AML1–ETO9a fusion protein (6, 7), and this effect was also observed in panobinostat-treated A/E9a;NRAS^{G12D};*Ifnar1*$^{-/-}$ cells, indicating that certain biochemical effects mediated by panobinostat remained unaffected by knockout of *Ifnar1* (Fig. 2C). Moreover, panobinostat caused a decrease in BrdU incorporation in both A/E9a;NRAS^{G12D} and A/E9a;NRAS^{G12D};*Ifnar1*$^{-/-}$ leukemias following treatment of tumor-bearing

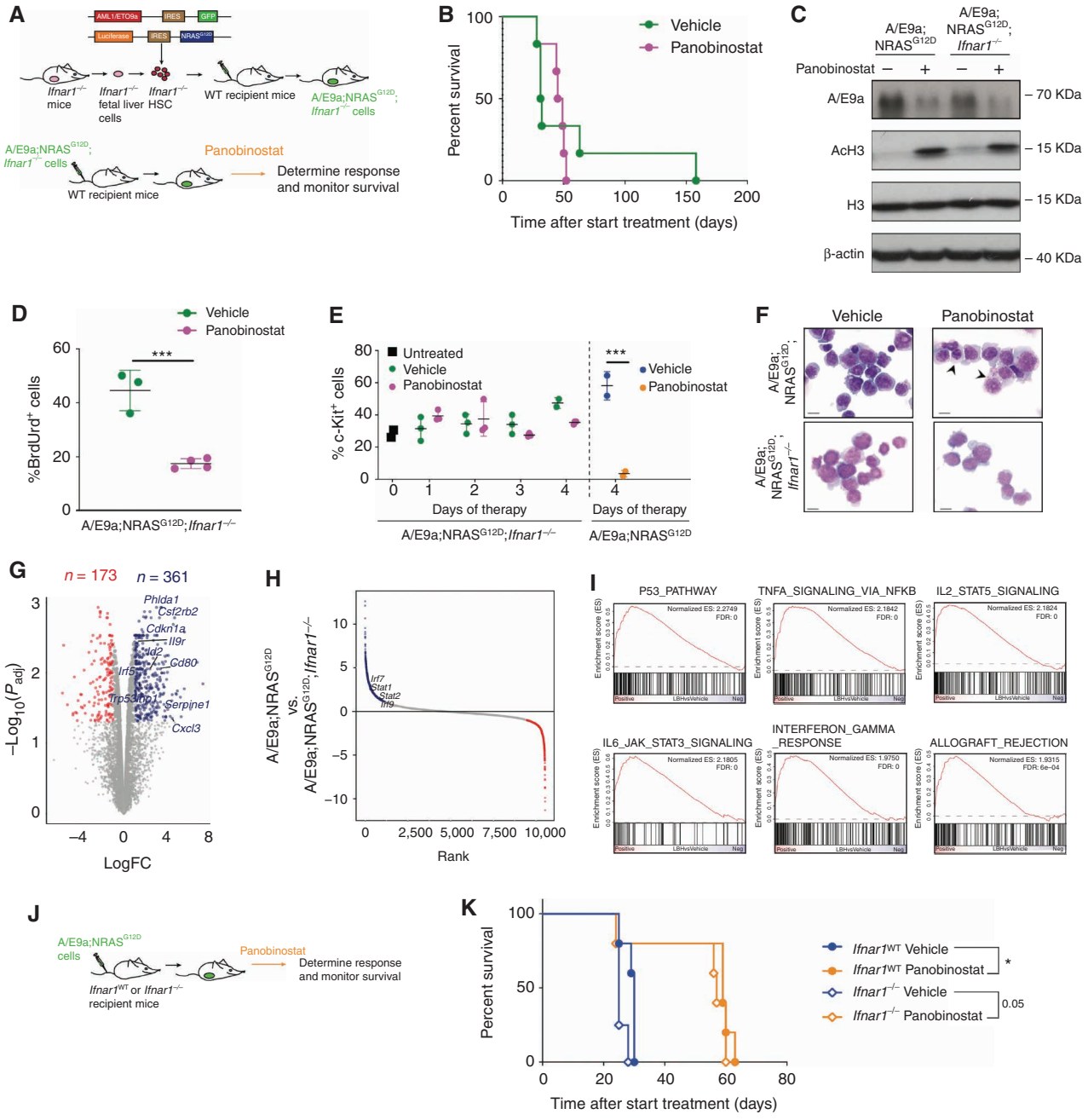

Figure 2. Expression of IFNAR on tumor cells is critical for the therapeutic efficacy of panobinostat. **A,** Schematic representation of the generation of A/E9a;NRAS^{G12D};*Ifnar1*$^{-/-}$ leukemias in wild-type (WT) recipient mice. **B,** Kaplan–Meier survival curves of mice bearing A/E9a;NRAS^{G12D};*Ifnar1*$^{-/-}$–driven leukemias treated with either vehicle or panobinostat ($n = 6$ mice/group). **C,** Representative immunoblot of WT (A/E9a;NRAS^{G12D}) or IFNAR-deficient (A/E9a;NRAS^{G12D};*Ifnar1*$^{-/-}$) cells treated with either vehicle of panobinostat for 24 hours *in vitro* for the AML1–ETO9a (AE9a) fusion protein; acetylated histone 3 (AcH3); total histone 3 (H3) and α-actin as loading control ($n = 3$). **D,** Cell-cycle analysis of A/E9a;NRAS^{G12D};*Ifnar1*$^{-/-}$ leukemia cells within the bone marrow of mice treated with vehicle or panobinostat. The percentage of cells in S-phase (BrdU^{+} cells) was determined by flow cytometry ($n = 3$–4; ***, $P < 0.001$). **E,** Flow cytometry analysis of the cell-surface expression of c-Kit on A/E9a;NRAS^{G12D};*Ifnar1*$^{-/-}$ tumor cells isolated from the bone marrow of mice treated for 4 days with vehicle or panobinostat. The differential expression of c-Kit on WT (A/E9a;NRAS^{G12D}) tumor cells at day 4 is shown for comparison ($n = 3$ mice/timepoint; ***, $P < 0.001$). **F,** Representative images of May-Grünwald/Giemsa-stained WT (A/E9a;NRAS^{G12D}) or IFNAR-deficient (A/E9a;NRAS^{G12D};*Ifnar1*$^{-/-}$) tumor cells isolated from the bone marrow of mice treated with vehicle or panobinostat for 4 days. Arrows indicate condensation of nuclear chromatin and appearance of azurophilic cytoplasmic granules, indicating myeloid differentiation (600× magnification; scale bar, 10 μm; $n = 3$). **G,** Volcano plot showing DEG (logFC > 1; $P_{adj} < 0.05$) between IFNAR-deficient (A/E9a;NRAS^{G12D};*Ifnar1*$^{-/-}$) leukemia cells isolated from panobinostat-treated and vehicle-treated leukemia-bearing mice. **H,** Comparison of DEG between panobinostat-treated and vehicle-treated WT (A/E9a;NRAS^{G12D}) and IFNAR-deficient (A/E9a;NRAS^{G12D};*Ifnar1*$^{-/-}$) tumor cells. **I,** GSEA of upregulated genes shown in **G**. **J,** Schematic representation of the generation of WT A/E9a;NRAS^{G12D} leukemias in *Ifnar1*^{WT} or *Ifnar1*$^{-/-}$ recipient mice. **K,** Kaplan–Meier survival curves of *Ifnar1*^{WT} or *Ifnar1*$^{-/-}$ mice bearing WT A/E9a;NRAS^{G12D}-driven leukemias treated with vehicle or panobinostat ($n = 5$ mice/group).

mice with panobinostat for 3 days (Fig. 2D). The ability of A/E9a;NRAS^{G12D};*Ifnar1*$^{-/-}$ tumors to differentiate in response to panobinostat was determined through assessment of cell-surface expression of c-Kit on tumor cells within the bone marrow over 4 days of therapy. There was insignificant alteration in c-Kit expression on panobinostat-exposed A/E9a;NRAS^{G12D};*Ifnar1*$^{-/-}$ cells in contrast to the significant decrease in c-Kit expression observed in A/E9a;NRAS^{G12D} leukemias exposed to panobinostat (Fig. 2E). Moreover, exposure of A/E9a;NRAS^{G12D};*Ifnar1*$^{-/-}$ leukemias to panobinostat *in vivo* did not induce morphologic changes consistent with myeloid differentiation such as condensation of nuclei and formation of cytoplasmic granules seen in panobinostat-treated A/E9a;NRAS^{G12D} cells (Fig. 2F). RNA-seq on A/E9a;NRAS^{G12D};*Ifnar1*$^{-/-}$ leukemias harvested from mice treated with panobinostat for 3 days was performed to determine if IFNAR deficiency affected the type I IFN response following treatment of A/E9a;NRAS^{G12D} cells with panobinostat (Supplementary Fig. S2C). This revealed 534 DEG between panobinostat-treated and vehicle-treated A/E9a;NRAS^{G12D};*Ifnar1*$^{-/-}$ tumor cells (logFC > 1, $P_{adj} < 0.05$; Fig. 2G; Supplementary Table S2). Comparison of the transcriptional changes observed in panobinostat-treated A/E9a;NRAS^{G12D} and A/E9a;NRAS^{G12D};*Ifnar1*$^{-/-}$ leukemias revealed that transcripts related to type I IFN signaling pathway, such as *Irf7*, *Irf9*, *Stat1*, and *Stat2*, were upregulated only in A/E9a;NRAS^{G12D} cells (Fig. 2H). GSEA and GO analysis of the 361 upregulated genes in panobinostat-treated A/E9a;NRAS^{G12D};*Ifnar1*$^{-/-}$ cells showed enrichment in the p53 pathway, IFNγ response, and cytokine signaling (Fig. 2G and I; Supplementary Fig. S2D), similar to A/E9a;NRAS^{G12D} cells (Fig. 1G). However pathways induced by type I IFN, observed in the panobinostat-treated A/E9a;NRAS^{G12D} leukemias, were not found in treated A/E9a;NRAS^{G12D};*Ifnar1*$^{-/-}$ cells. Our results indicate that panobinostat-mediated partial degradation of A/E9a and induction of cell-cycle arrest are not sufficient to induce leukemia differentiation; in contrast, activation of the IFNAR pathway on the tumor cells mediates their myeloid differentiation and is critical for the therapeutic effect of panobinostat.

Given that signaling through IFNAR expressed on A/E9a;NRAS^{G12D} leukemias was important for a prolonged therapeutic response to panobinostat *in vivo*, the role of type I IFN signaling in the host cells in this context was determined. Wild-type C57BL/6 (*Ifnar1*^{WT}) and *Ifnar1*$^{-/-}$ mice on a C57BL/6 background (*Ifnar1*$^{-/-}$) were transplanted with A/E9a;NRAS^{G12D} leukemias and treated with vehicle or panobinostat (Fig. 2J). The therapeutic effect of panobinostat against A/E9a;NRAS^{G12D} leukemias was equivalently strong in mice with (*Ifnar1*^{WT}) or without (*Ifnar1*$^{-/-}$) a host type I IFN response (Fig. 2K; Supplementary Fig. S2E). These results highlight the importance of tumor-intrinsic type I IFN signaling for panobinostat-mediated differentiation and therapeutic efficacy.

Single-Cell Analysis Identifies Activation of the Type I IFN Pathway in DCs in Response to Panobinostat

Treatment of cancer cells with certain epigenetic drugs such as DNA methyltransferase inhibitors (DNMTi) can induce a molecular and biological response that mimics antiviral responses through reactivation of silenced endogenous retroviruses (ERV), resulting in production of type I IFN by the tumor cells (21–23). Given that A/E9a;NRAS^{G12D} cells exposed to panobinostat displayed a type I IFN transcriptional response, we determined if IFN was being produced by the treated leukemias. No increase in *Ifna* or *Ifnb* transcription in A/E9a;NRAS^{G12D} cells was detected in response to panobinostat by genome-wide analysis using microarrays (FC >1.5, $P < 0.05$; Supplementary Fig. S3A) or gene-specific qRT-PCR (Supplementary Fig. S3B). In the absence of evidence for production of type I IFN by the A/E9a;NRAS^{G12D} leukemias in response to panobinostat, we sought to identify the source. Interestingly, we did not detect either IFNα or IFNβ in the serum of panobinostat-treated mice, suggesting that induction of type I IFN in response to panobinostat occurred locally rather than systemically in the tissues. We ruled out IFN production being mediated by the stroma, because stromal cells from leukemia-bearing mice in fact downregulated type I IFN genes in response to panobinostat (Supplementary Fig. S3C and S3D). We then focused on DCs, which are capable of secreting IFNα and IFNβ in response to infection (24). These cells are phenotypically divided into pDCs (CD11c^{int}Siglec-H^{+}), which produce high amount of type I IFN and other cytokines in response to pathogens (25), and conventional DCs (cDC; CD11c^{hi}Siglec-H^{-}), which activate T cells and can further be divided into cDC1 and cDC2, depending on their function and developmental origin (26).

To simultaneously examine the composition and transcriptional responses of all DC subsets, single-cell CITE-seq and the related cell hashing method (27, 28) were performed on DCs isolated from vehicle- or panobinostat-treated mice bearing A/E9a;NRAS^{G12D} leukemias (Fig. 3A; Supplementary Fig. S4A). Concurrent experiments were performed on wild-type (leukemia-free) mice to obtain baseline DC transcriptome information and content levels. Transcriptomes of single cells were generated and Hashtag oligonucleotide (HTO) classification allowed the identification of the different samples (Supplementary Fig. S4B; Supplementary Table S3). Unsupervised clustering defined 13 distinct clusters (Supplementary Fig. S4C), which were assigned to the different DC subpopulations previously described (26, 29) by combining the transcriptional profile (Supplementary Fig. S4D and S4E; Supplementary Table S4) with detection of cell-surface markers CD11c and Siglec-H using antibody-derived tags (ADT; Supplementary Fig. S4F). pDCs, cDC1s, cDC2s, CCR7^{hi} DCs (29–31), and monocyte-derived DCs (moDC) were identified in samples from leukemia-free and leukemia-bearing C57BL/6 mice visualized using Uniform Manifold Approximation and Projection (UMAP; ref. 32; Fig. 3B). Calculation of the relative proportion of each DC subset identified an expansion of the pDC compartment in leukemia-bearing mice, with 40% pDCs in vehicle-treated mice transplanted with A/E9a;NRAS^{G12D} cells compared with 12% pDCs in vehicle-treated leukemia-free mice (Fig. 3C). We confirmed this significant increase in pDCs in tumor-bearing mice by flow cytometry (Fig. 3D). Interestingly, the DC composition in panobinostat-treated A/E9a;NRAS^{G12D} mice was restored to approximate that in vehicle-treated leukemia-free mice through the reduction in pDC numbers (Fig. 3C). We observed a similar

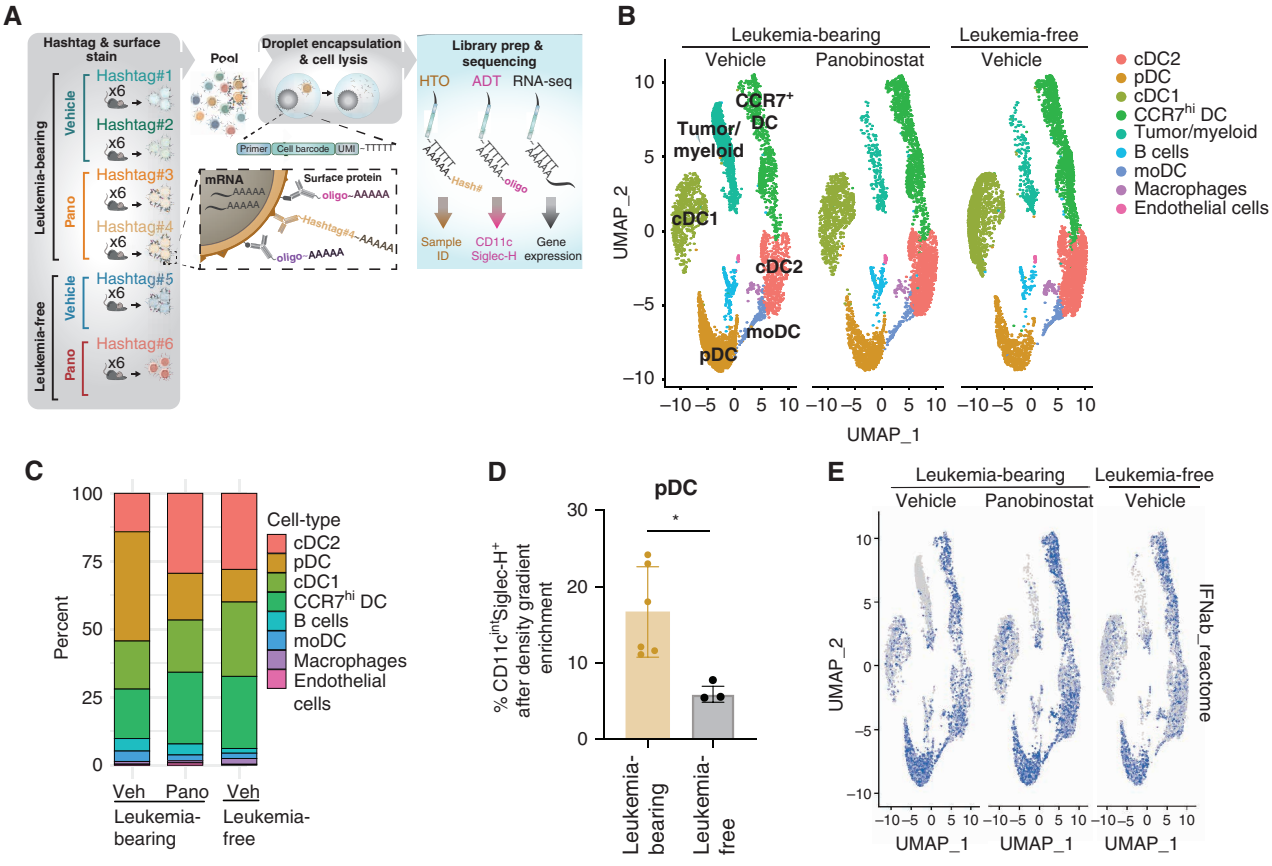

Figure 3. Single-cell analysis identifies activation of the type I IFN pathway in DCs in response to panobinostat. **A,** Experimental setup for CITE-seq and Cell Hashing on DCs isolated from A/E9a;NRAS^{G12D} leukemia-bearing or leukemia-free mice treated with vehicle or panobinostat for 2 days. **B,** Annotated cell clusters based on RNA expression. **C,** Relative frequency of individual clusters, excluding tumor/myeloid cells. **D,** Percentage of pDCs (CD11c^{int}Siglec-H^{+}), after density gradient enrichment, in the spleen of vehicle-treated leukemia-free ($n = 3$ experiments) and leukemia-bearing mice ($n = 6$ experiments) 2 days after treatment with vehicle. In the case of leukemia-bearing mice, we also excluded GFP^{+} leukemia cells to calculate the percentage of pDC. **E,** Activity of type I IFN signature on single-cell clusters. **F,** AUCell enrichment score of type I IFN signature in DC subpopulations (**, $P < 0.01$; ***, $P < 0.001$).

trend in panobinostat-treated leukemia-free mice compared with vehicle-treated animals (Supplementary Fig. S4G). The AUCell algorithm (33) identified that pDCs, CCR7^{hi} DCs, and to a lesser extent cDCs, were enriched in genes from the REACTOME IFNα/β signaling, which include *Ifnα* and *Ifnβ,* and IFN-stimulated genes (ISG; Fig. 3E). Treatment of mice bearing A/E9a;NRAS^{G12D} leukemias with panobinostat resulted in an increase in the type I IFN signature in pDC and CCR7^{hi} DC populations (Fig. 3F).

Type I IFN Is Produced by pDCs within the Tumor Microenvironment in Response to Panobinostat

To confirm which cell type was producing type I IFN in response to panobinostat, pDCs and cDCs were isolated from vehicle- and panobinostat-treated A/E9a;NRAS^{G12D}-bearing mice (Fig. 4A). Panobinostat treatment significantly induced the transcription of both *Ifna4* and *Ifnb1* genes in pDCs from leukemia-bearing mice (Fig. 4B). In contrast, cDCs from leukemia-bearing mice did not upregulate type I IFN in response to panobinostat (Fig. 4C). The ability of panobinostat to induce type I IFN production from pDCs was further demonstrated using *ex vivo* pDCs from IFNβ/YFP reporter mice that had been cotreated with Toll-like receptor agonists poly I:C or CpG (Supplementary Fig. S5A). Induction of the IFNβ/YFP reporter was detected as early as 12 hours after incubation with panobinostat, indicating that HDAC inhibition can induce *Ifnβ* mRNA expression in isolated pDCs. These results suggest that panobinostat activates pDCs to produce type I IFN, which leads to pDC apoptosis, and reduced numbers (Fig. 3C), as it has been shown during viral infections and administration of Toll-like receptor ligands (34).

To investigate the functional role of pDCs in mediating the antitumor response to panobinostat, an anti-PDCA1

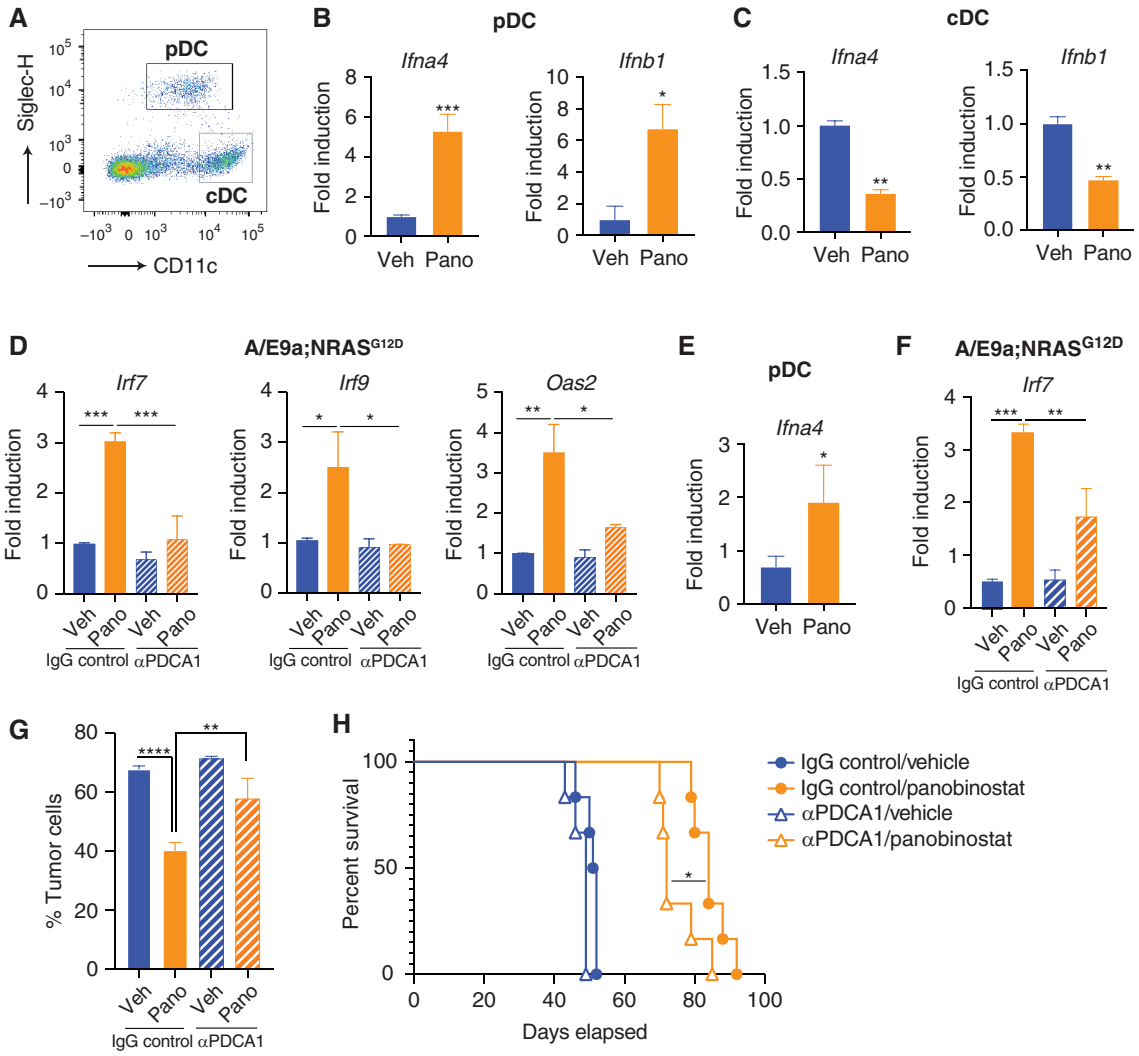

Figure 4. Type I IFN is produced by pDCs within the tumor microenvironment in response to panobinostat. **A,** Flow cytometry gating strategy, after density gradient enrichment and exclusion of GFP+ leukemia cells, to isolate pDCs and cDCs from the spleen of mice bearing A/E9a;NRAS^{G12D}-driven leukemias. **B** and **C,** qRT-PCR of *Ifna4* and *Ifnb1* transcripts in pDCs (**B**) and cDCs (**C**) isolated from the spleen of mice bearing A/E9a;NRAS^{G12D}-driven leukemias treated with either vehicle or panobinostat following 5 days of therapy (*, $P < 0.05$; **, $P < 0.01$). **D,** qRT-PCR of *Irf7* transcript in A/E9a;NRAS^{G12D} tumor cells isolated from the spleen of mice receiving IgG control or anti-PDCA1 and treated with either vehicle or panobinostat following 3 days of therapy (**, $P < 0.01$). **E,** qRT-PCR of *Ifna4* in pDCs isolated from the bone marrow of mice bearing A/E9a;NRAS^{G12D}-driven leukemias treated with either vehicle or panobinostat following 3 days of therapy (*, $P < 0.05$). **F,** qRT-PCR of *Irf7* transcript in A/E9a;NRAS^{G12D} tumor cells isolated from the bone marrow of mice receiving IgG control or anti-PDCA1 and treated with either vehicle or panobinostat following 5 days of therapy (**, $P < 0.01$; ***, $P < 0.001$). **G,** Percentage of tumor cells in the bone marrow of mice bearing A/E9a;NRAS^{G12D}-driven leukemias receiving IgG control or anti-PDCA1 and treated with either vehicle or panobinostat for 5 days (**, $P < 0.01$; ****, $P < 0.0001$). **H,** Kaplan–Meier survival curves of mice bearing A/E9a;NRAS^{G12D}-driven leukemias receiving IgG control or anti-PDCA1 and treated with either vehicle or panobinostat ($n = 6$ mice/group; *, $P < 0.05$).

antibody was used to deplete pDCs *in vivo* (Supplementary Fig. S5B). Mice bearing A/E9a;NRAS^{G12D} leukemias were injected with a control antibody or pDC-depleting antibody, and these mice were treated with vehicle or panobinostat for 3 days before leukemias were harvested. As shown in Fig. 4D, upregulation of type I IFN-response genes, such as *Irf7*, *Irf9*, and *Oas2*, in A/E9a;NRAS^{G12D} cells in response to panobinostat was almost completely abrogated in the absence of pDCs. We also analyzed the bone marrow of tumor-bearing mice and found that, similar to splenic pDCs, the pDCs present in the bone marrow upregulated the expression of type I IFN in response to panobinostat (Fig. 4E). Tumor cells in the bone marrow of panobinostat-treated mice showed increased expression of *Irf7*, which was impaired in pDC-depleted mice (Fig. 4F; Supplementary Fig. S5C). Importantly, the beneficial therapeutic effect of panobinostat was affected by the absence of pDCs, with significantly higher tumor burden in panobinostat-treated mice receiving anti-PDCA1 compared with control antibody (Fig. 4G). Moreover, depletion of pDCs from mice transplanted with A/E9a;NRAS^{G12D} cells resulted in a significant reduction in therapeutic efficacy mediated by panobinostat, with a lower median survival of 72 days in mice receiving anti-PDCA1 compared with 84 days for IgG control mice

(Fig. 4H). Taken together, these data reveal that panobinostat-mediated type I IFN production by pDCs is important for the IFN response observed in A/E9a;NRAS^{G12D} cells as well as for the antileukemia effects of panobinostat. Although we focused on the role of pDCs, other immune cells are probably important, as panobinostat treatment of leukemia-bearing immune-deficient mice (NSG; median survival = 28 days) was less effective than in immune-competent mice (C57BL/6, median survival = 52 days; Supplementary Fig. S5D).

Panobinostat Induces Transcriptional Activation of Type I IFN Genes in pDCs through Increased Histone Acetylation

The production of type I IFN in response to epigenetic drugs has been proposed to be triggered by the formation of double-stranded RNA (dsRNA) derived from ERVs, which once in the cytoplasm are sensed by pattern-recognition receptors and lead to IRF7 activation through mitochondrial antiviral-signaling protein (MAVS; ref. 23). Accordingly, the effect of panobinostat on dsRNA accumulation in pDCs was assessed. There was no detectable dsRNA in the cytoplasm of FLT3L-derived pDCs incubated with panobinostat or vehicle (Supplementary Fig. S6A), suggesting an alternative mechanism for the induction of type I IFN in panobinostat-treated pDCs. A previous study showed that HDAC inhibition in a mouse fibroblast cell line can result in derepression of the *Ifnb1* promoter, leading to enhanced production of endogenous IFN (35). To determine if exposure of pDCs and cDCs to panobinostat resulted in increased acetylation at the regulatory regions controlling the expression of IFN genes, chromatin immunoprecipitation followed by sequencing (ChIP-seq) studies were performed probing for H3K27 acetylation (H3K27Ac). A genome-wide increase in H3K27Ac levels was observed in pDCs harvested from panobinostat-treated mice bearing A/E9a;NRAS^{G12D} leukemias compared with vehicle-treated mice. Interestingly, analysis of cDCs harvested from the same microenvironment showed a slight decrease in H3K27Ac following exposure to panobinostat (Fig. 5A). In addition, assays for transposase-accessible chromatin by sequencing (ATAC-seq; ref. 36) were performed using pDCs and cDCs harvested from transplanted mice to correlate potential panobinostat-induced changes in chromatin accessibility with transcriptional activity. Interestingly, there were few significant genome-wide changes in accessible regions after panobinostat treatment in pDCs or cDCs (Fig. 5B).

Analysis of transcriptional changes mediated by panobinostat in pDCs and cDCs isolated from leukemia-bearing mice, using low input bulk RNA-seq (Supplementary Fig. S6B), demonstrated 1,665 DEG in pDCs and only 323 DEG cDCs (Fig. 5C; Supplementary Tables S5 and S6). Importantly, an increase in *Ifnb1* transcription was detected in pDCs but not in cDCs following exposure to panobinostat (Fig. 5C), confirming the results obtained by RT-PCR (Fig. 4A and B). GSEA and GO analysis on the 725 genes upregulated in pDCs exposed to panobinostat found enrichment in the G_2–M checkpoint pathway, E2F targets, metabolic and cytokine production pathways, including type I IFN response (Fig. 5D; Supplementary Fig. S6C). Parallel analysis on the 168 genes upregulated by panobinostat in cDCs showed enrichment in pathways induced by IFNα and IFNβ, as well as IFNγ response (Fig. 5E; Supplementary Fig. S6D), similar to A/E9a;NRAS^{G12D} tumor cells (Fig. 1G). These results suggest that pDCs in the tumor microenvironment are activated by panobinostat to produce type I IFN, which then signals through IFNAR on pDCs, cDCs, and A/E9a;NRAS^{G12D} leukemia cells.

To definitively determine whether panobinostat resulted in acetylation of the accessible chromatin regions of type I IFN genes in pDCs, leading to their transcriptional activation, the H3K27Ac ChIP-seq, ATAC-seq, and bulk RNA-seq profiles for type I IFN genes were overlapped in pDCs, and cDCs as comparison. A clear increase in H3K27Ac at the *Ifnβ1* gene (Fig. 5F) and more generally in the cluster of type I IFN genes (Fig. 5G) was detectable in pDCs harvested from panobinostat-treated leukemia-bearing mice (orange profiles), compared with pDCs from vehicle-treated mice (blue profiles). Enhanced H3K27Ac at type I IFN gene loci observed in pDCs exposed to panobinostat correlated with increased transcription of the corresponding genes based on mRNA reads, and overlapped with open chromatin regions (Fig. 5F and G). In contrast, analysis of cDCs showed that panobinostat treatment barely affected H3K27Ac levels at type I IFN genes, and little if any detectable increase in transcription of those genes was observed (Fig. 5F and G). Interestingly, low-level H3K27Ac marks and mRNA reads were observed in pDCs, but not in cDCs, from vehicle-treated mice (Fig. 5F and G), suggesting that pDCs are epigenetically and transcriptionally primed to produce type I IFN.

Panobinostat Enhances the Connectivity of Core Transcription Factors in pDCs

The data detailed above indicated that despite both pDCs and cDCs demonstrating open chromatin regions around type I IFN genes, only pDCs were putatively primed to produce type I IFN following exposure to panobinostat (Fig. 5F and G). It is possible that these differences were due to the expression and/or activity of core transcription factors (TF) distinct for each cell type. To test this hypothesis, the information derived from H3K27Ac ChIP-seq studies on vehicle-treated pDCs and cDCs was used to define the enhancer landscape of each cell type. This allows the identification of superenhancers (SE), broad open regions of chromatin with high levels of H3K27Ac that facilitate binding of the core TFs that control the transcriptional program of a given cell (37, 38). SEs for pDCs and cDCs were defined by stitching H3K27Ac peaks within 12.5 Kb in each cell type and ranking them by H3K27Ac signal (Supplementary Fig. S7A). Subsequent identification of SE target genes revealed 584 in pDCs and 299 in cDCs, with only 16% shared between both populations (Supplementary Fig. S7B; Supplementary Table S7). TFs associated with SEs were identified, and open regions within such SEs were used to identify TF motifs and create TF-binding networks [i.e., core regulatory circuitries (CRC)] for pDCs and cDCs using COLTRON (https://pypi.python.org/pypi/coltron; Supplementary Fig. S7C). Importantly, when the CRC of pDCs and cDCs were overlapped, only 9 shared core TFs were identified (Fig. 6A). Overall TF connectivity in the network was visualized by calculating the number

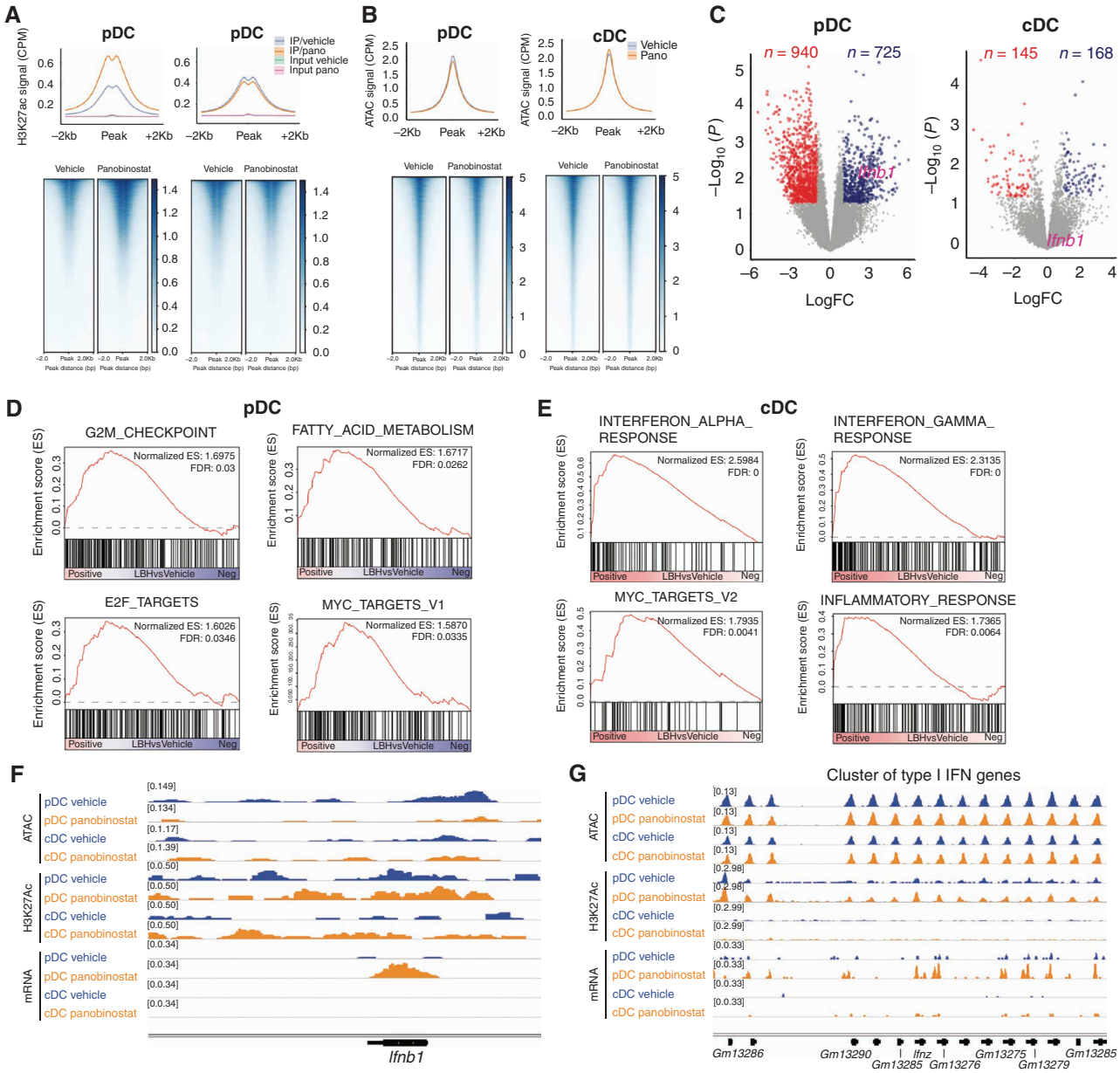

Figure 5. Panobinostat induces transcriptional activation of type I IFN genes in pDCs through increased histone acetylation. **A,** H3K27Ac ChIP-seq on pDCs and cDCs isolated from A/E9a;NRAS^{G12D} leukemia-bearing mice treated with vehicle or panobinostat for 2 days. **B,** ATAC-seq on pDCs and cDCs isolated from A/E9a;NRAS^{G12D} leukemia-bearing mice treated with vehicle or panobinostat for 2 days. **C,** Volcano plot showing DEG (logFC > 1; $P < 0.05$) between panobinostat-treated and vehicle-treated pDCs (left) and cDCs (right) isolated from A/E9a;NRAS^{G12D} leukemia-bearing mice. **D,** GSEA of upregulated genes in pDCs shown in **C**. **E,** GSEA of upregulated genes in cDCs shown in **C**. **F** and **G,** Read-density tracks of normalized ATAC-seq, H3K27Ac ChIP-seq, and RNA-seq at the *Ifnβ1* locus (**F**) and *Ifnα* loci (**G**) in pDCs and cDCs isolated from A/E9a;NRAS^{G12D} leukemia-bearing mice treated with vehicle or panobinostat for 2 days.

of TF motifs within the SE of a node TF (inward binding) and the number of TF-associated SEs bound by a node TF (outward binding; refs. 37–39; Fig. 6B). Among the most connected core TFs in pDCs were TCF4, IRF1, and IRF8, previously described as important for pDC development and function (40, 41), and known factors associated with B-cell lineage, including SPIB and FOXP1 (Fig. 6B). This was further confirmed when the clique fraction of the core TFs (see Methods) was calculated, and SPIB, FOXP1, IRF8, and IRF1 were TFs identified to dominate clique membership in pDCs (Fig. 6C). Importantly, both IRF1 and IRF8 have been shown to be involved in type I IFN-mediated responses (41, 42). As an orthogonal approach, single-cell RNA-seq data from Fig. 3 was utilized. AUCell analysis confirmed that the pDC and cDC signatures defined by COLTRON were active in pDC and cDC subsets, respectively, defined at the single-cell level (Supplementary Fig. S7D), thus validating the regulatory networks established using COLTRON.

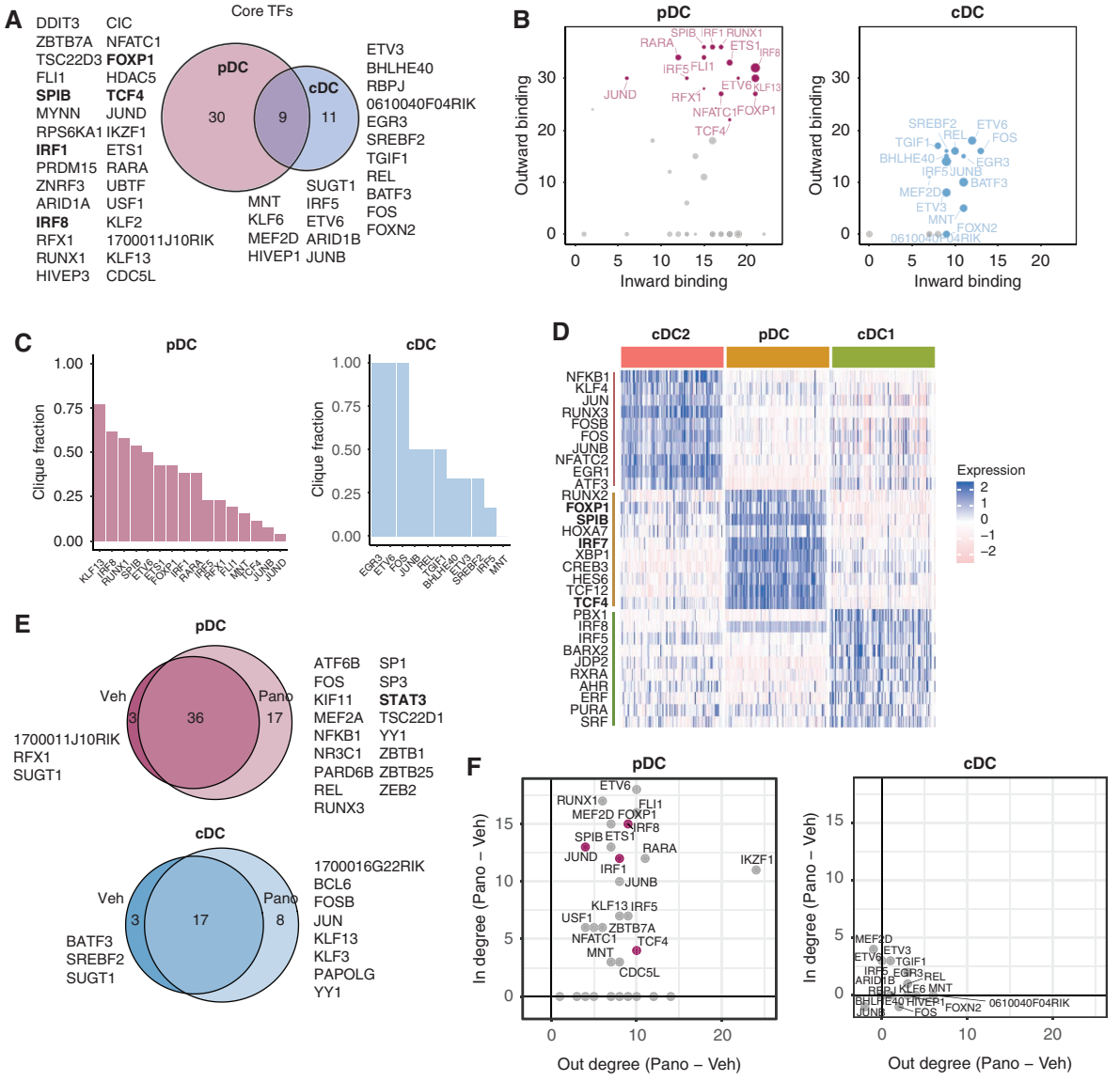

Figure 6. Panobinostat enhances the connectivity of core TFs in pDCs. **A,** Venn diagram showing core TFs in pDCs and cDCs. **B,** Inward/outward binding plots of pDCs and cDCs, with highly connected core TFs highlighted. **C,** Clique fraction for highly connected core TFs in pDCs and cDCs. **D,** Core TFs defining cell identity for pDCs, cDC1, and cDC2 based on SCENIC analysis on single-cell data. **E,** Venn diagram showing core TFs in panobinostat-treated and vehicle-treated pDCs and cDCs. **F,** Difference in inward/outward binding between panobinostat-treated and vehicle-treated pDCs and cDCs.

Application of the single-cell regulatory network inference and clustering (SCENIC) algorithm, which infers regulatory networks based on predicted TF activity (33), was used to explore in more detail the CRC of pDCs, cDC1s, and cDC2s. Clustering using SCENIC (Supplementary Fig. S7E) identified the same cell types as clustering based only in the transcriptional profile (Fig. 3B). The TFs driving the identity of each cell type were then identified (Fig. 6D; Supplementary Table S8), revealing TCF4, FOXP1, SPIB, and IRF7, the master regulator of type I IFN-dependent response (43), in pDCs which were not present in cDC1 or cDC2 clusters (Fig. 6D). This analysis also showed IRF8 as a SCENIC marker for pDCs and cDC1s (Fig. 6D). These results indicate that the unique capacity of pDCs to produce IFN in response to panobinostat likely relies on their dependency for cell identity on IRFs, which are known to be essential for the transcriptional activation of type I IFN genes. To further confirm this hypothesis, we determined the CRC of pDCs and cDCs after panobinostat treatment. As shown in Fig. 6E and Supplementary Table S9, there were 17 new core TFs used by pDCs in response to HDAC inhibition, including STAT3, which is known to regulate the expression of ISGs (44). Importantly, panobinostat increased in pDCs, but not in cDCs, the connectivity of core TFs (FOXP1, SBIP, TCF4, IRF4, and IRF8), indicating enhanced interaction between these TFs in response to panobinostat (Fig. 6F). To our knowledge, the present study is the first to describe the CRC for pDCs and cDCs, identifying the TF interactions that regulate the transcriptional program in each cell type before and after treatment. In addition, these data support a different origin

for pDCs and cDCs, with pDCs closer to the B-cell lineage, as has been recently proposed (45).

Combining Panobinostat and Recombinant Type I IFN Enhances Myeloid Differentiation and Improves Therapeutic Efficacy in Mouse and Human AML

Given the results linking activation of type I IFN signaling to panobinostat-mediated differentiation of A/E9a;NRAS^{G12D} cells and the therapeutic efficacy of panobinostat in this setting, the combination of panobinostat and recombinant IFNα1 (rIFNα1) was tested in leukemia-bearing mice. To determine the effect of this combination on myeloid differentiation, CD11b expression on the tumor cells following 4 days of therapy was assessed. In contrast to single-agent panobinostat treatment, rIFNα1 alone had no effect on the myeloid differentiation status of these cells. The combination of rIFNα1 with panobinostat resulted in an increase in CD11b expression that did not reach statistical significance (Fig. 7A). More importantly, although rIFNα1 had no therapeutic benefit in mice bearing A/E9a;NRAS^{G12D} leukemias, the combination of rIFNα1 and panobinostat resulted in a significant increase in the survival of tumor-bearing mice compared with those mice treated with panobinostat alone. The median survival benefit of panobinostat + rIFNα1 over vehicle was 79.5 days, compared with 32.5 days for single-agent panobinostat treatment over vehicle (Fig. 7B). We also tested the efficacy of the combinatorial treatment in MLL-driven leukemias. Treatment of M/A;NRAS^{G12D} leukemias with panobinostat and type I IFN induced higher expression of Sca-1 compared with panobinostat alone (Supplementary Fig. S8A) and was concomitant with a significant survival advantage *in vivo*, with a median survival of 18 days for mice receiving panobinostat + rIFNβ, compared with 16 days for vehicle-treated and 15 days for rIFNβ-treated mice (Supplementary Fig. S8B). As we previously showed (7), we found no survival advantage after panobinostat treatment alone (median survival = 16 days), probably due to the more aggressive nature of leukemias with MLL fusion proteins.

To determine the relevance of combining panobinostat and type I IFN to treat human leukemia, we established primary patient-derived xenografts (PDX) with t(8;21) AML cells. We treated tumor-bearing mice for 4 weeks with vehicle, rIFNα2 (isoform used clinically), panobinostat, or panobinostat + rIFNα2a, analyzing the bone marrow at days 14, 28, and 42 after starting the treatment (Fig. 7C). We first confirmed the presence of the t(8;21) translocation in the engrafted leukemia cells (Supplementary Fig. S8C). There was a significant upregulation of CD11b in the leukemic cells (CD45$^+$CD3^{neg}HLA-DR$^+$) after 14 days of treatment with panobinostat + rIFNα2a compared with treatment with panobinostat or rIFNα2a alone (Fig. 7D; Supplementary Fig. S8D). Importantly, this myeloid differentiation induced by the combination of panobinostat and type I IFN on tumor cells at day 14 correlated with a reduction in the leukemia burden (CD45$^+$CD3^{neg}) at day 28, which was significant at day 42 (Fig. 7E). In contrast, there was no reduction in tumor burden in mice treated only with panobinostat, and a significant increase in leukemia cells over time was observed in untreated mice (vehicle) and rIFNα2a-treated mice (Fig. 7E). We confirmed the enhanced therapeutic efficacy of the combinatorial therapy to treat t(8;21) AML using cell-derived xenograft (CDX) models established with Kasumi-1 cells. A significant reduction of tumor cells was observed after treatment with panobinostat + rIFNα2a, based on reduced bioluminescence signal [area-under-curve (AUC); Supplementary Fig. S8E and S8F] and a decrease in CD34$^+$CD45$^+$ cells in the bone marrow (Supplementary Fig. S8G) compared with vehicle-treated mice. We also characterized the response to the combinatorial therapy in a human PDX model of *NRAS*^{mut} AML. Similar to t(8;21) AML, we observed a significant increase in CD11b on tumor cells (CD45$^+$CD34^{neg}) after treatment with panobinostat + rIFNα2a compared with vehicle-treated mice (Fig. 7F), which correlated with a significant reduction in leukemia burden (Fig. 7G). Finally, to characterize the *in vivo* response to panobinostat of human pDCs, we established human cord blood–derived xenografts. Panobinostat treatment induced a significant decrease in mature pDCs in the bone marrow (Fig. 7H), similar to the effect of panobinostat on mouse pDCs (Fig. 3C). Collectively, these results highlight the therapeutic potential of combining HDACi and type I IFN as a new approach to treat AML.

DISCUSSION

As AML is characterized by deregulation of epigenetic modifications, which contribute to the pathogenesis of the disease, targeting the epigenome through the pharmacologic inhibition of epigenetic modifiers has been the main focus of many preclinical and clinical studies in leukemia during the last two decades (46). This previous work has clearly demonstrated that epigenetic drugs, such as HDACis and DNMTis, have multiple mechanisms of action that result in loss of leukemia cell proliferation and survival, including through the activation of the immune system (47). DNMTis have been shown to induce a type I IFN response, activating the IFNAR-mediated pathway, which can contribute to the antitumor effects of these anticancer agents (21, 22). However, these previous studies with epigenetic therapies focused on the pathways leading to type I IFN production by cancer cells, and the direct impact of these compounds within the immune compartment was not characterized. In this regard, recent evidence strongly indicates that epigenetic agents can also regulate the function of immune cells in the tumor microenvironment, and therefore they have the capacity to modulate the antitumor immune response (46, 47). Here we demonstrate that the panobinostat-mediated induction of type I IFN by host pDCs is required for the full therapeutic benefit of HDACis in preclinical models of t(8;21) AML (Fig. 7I). This novel immunomodulatory mechanism initiated by the effect of an epigenetic drug on immune cells, rather than the tumor, highlights the importance of understanding the global effects triggered by epigenetic therapies to maximize their therapeutic potential in the clinical setting.

Mechanistically, the IFN-inducing activity of panobinostat was specifically confined to pDCs, and the induction of type I IFN genes in these cells was concomitant with panobinostat-mediated hyperacetylation within the *Ifn* loci. The activation of type I IFN production occurred at

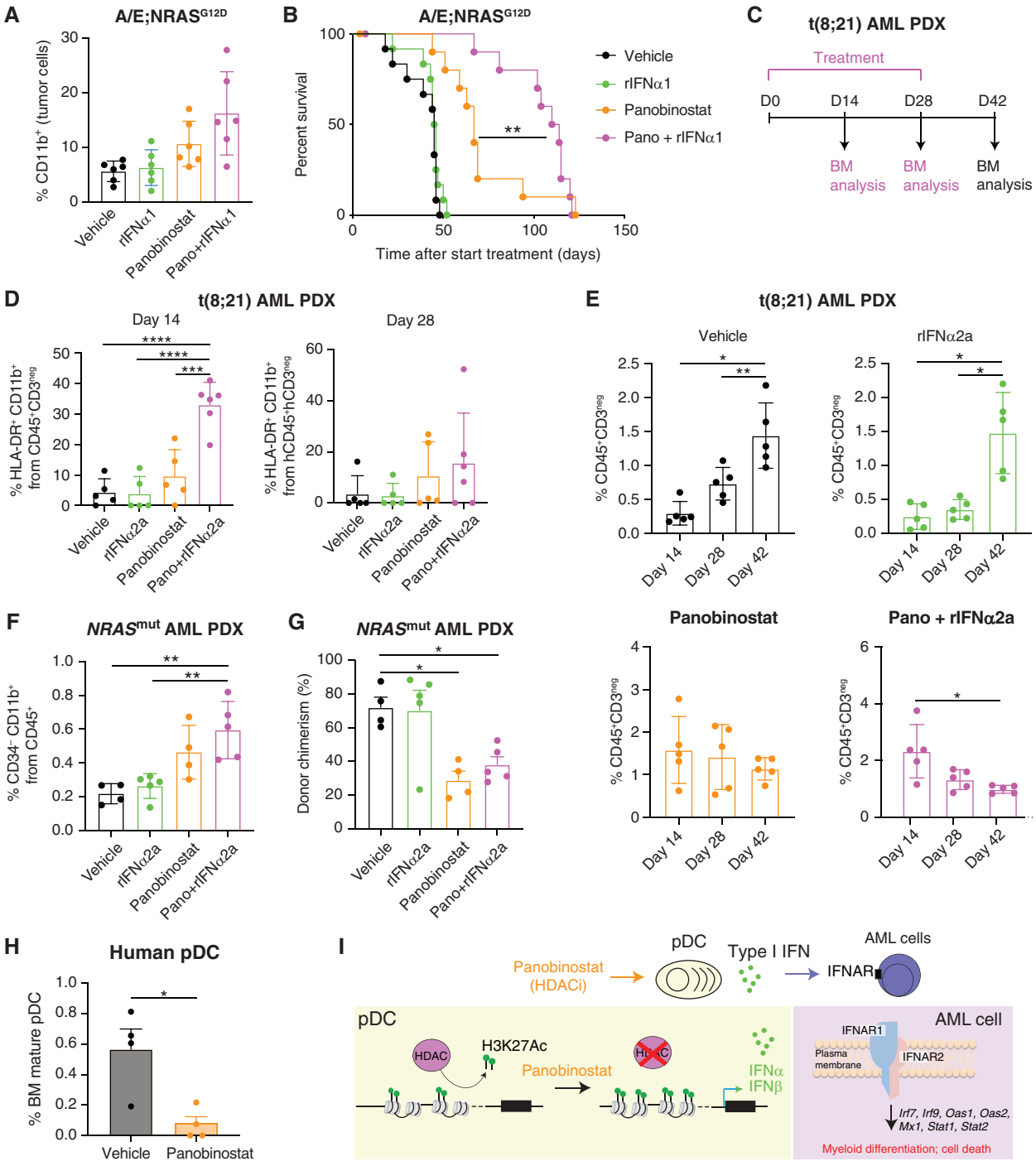

Figure 7. Combining panobinostat and type I IFN enhances myeloid differentiation and improves therapeutic efficacy in AML. **A,** Flow-cytometric analysis of the cell-surface expression of CD11b on A/E9a;NRAS^{G12D} tumor cells isolated from the bone marrow of mice treated for 4 days with vehicle, rIFNα1, panobinostat, or a combination of rIFNα1 + panobinostat ($n = 3$). **B,** Kaplan–Meier survival curves of mice bearing A/E9a;NRAS^{G12D}-driven leukemias treated with vehicle, rIFNα1, panobinostat, or the combination of rIFNα1 + panobinostat ($n = 11$–12 mice/group; **, $P < 0.005$). **C,** Schematic representation of the t(8;21) AML PDX experiment. **D,** Percentage of CD11b$^+$ HLA-DR$^+$ tumor cells (CD45$^+$CD3^{neg}) at day 14 and day 28 in the bone marrow of t(8;21) AML xenografts treated *in vivo* for 28 days with vehicle, panobinostat, rIFNα2, or panobinostat + rIFNα2. Gated on live/singlets/mCD45^{neg}cells ($n = 5$–6; ***, $P < 0.001$; ****, $P < 0.0001$). **E,** Percentage of tumor cells (CD45$^+$CD3^{neg}) at days 14, 28, and 42 in the bone marrow of t(8;21) AML xenografts treated *in vivo* for 28 days with vehicle, panobinostat, rIFNα2, or panobinostat + rIFNα2. Gated on live/singlets/mCD45^{neg} cells ($n = 5$; *, $P < 0.05$; **, $P < 0.01$). **F,** Percentage of CD11b$^+$CD34^{neg} tumor cells (CD45$^+$) in the bone marrow of *NRAS*^{mut} AML xenografts treated *in vivo* for 28 days with vehicle, panobinostat, rIFNα2, or panobinostat + rIFNα2 ($n = 5$; **, $P < 0.01$). Gated on viable/singlets/mCD45.1^{neg} cells. **G,** Percentage of donor chimerism (hCD45$^+$/hCD45$^+$ + mCD45.1$^+$) in the bone marrow of *NRAS*^{mut} AML PDX at day 28 after treatment with vehicle, panobinostat, rIFNα2, or panobinostat + rIFNα2 (*, $P < 0.05$). **H,** Percentage of mature pDCs (CD45$^+$Lin$^-$CD45RA$^+$HLA-DR$^+$CD123$^+$CD11c$^-$CD11b$^-$CD86^{hi}) in the bone marrow of NSG mice transplanted with human cord blood after 28 days treatment with panobinostat or vehicle (*, $P < 0.05$). Gated on live/singlets. **I,** Schematic model of the proposed mechanism of type I IFN expression induced by panobinostat in pDCs, leading to activation of IFNAR in AML cells, which induces their differentiation toward the myeloid lineage and subsequent cell death.

the transcriptional level through increased H3K27Ac and, therefore, is different from the viral mimicry mechanism proposed for other epigenetic inhibitors, which induce the expression of ERV-derived dsRNA that is detected by intracellular sensors, leading to type I IFN gene transcription (23). Interestingly, only pDCs but not cDCs responded to HDAC inhibition by upregulating transcription of type I IFN genes. We found that pDCs were in a preactivated state before treatment, with relatively high basal histone acetylation levels in type I IFN genes, influenced by the transcriptional dependency on IRFs that we have shown for pDCs and drives cell identity of this population. In line with this, previous work demonstrated that pDCs show high level of H3K27Ac in pDC-specific genes compared with other subtypes of DCs (monocyte-derived DCs), and this correlates with the expression of these cell type–specific genes (48). This basal high H3K27Ac is probably required for panobinostat to be able to increase histone acetylation level to drive cell type–gene expression, and that is the reason why panobinostat increases H3K27Ac only in pDCs.

We and others previously demonstrated that the use of HDACis in mouse models of t(8;21) AML resulted in leukemia cell differentiation, cell-cycle arrest, and apoptosis (7, 49–51). The results provided herein unveil that panobinostat also triggers a very strong activation of the IFNAR signaling pathway in leukemia cells, which is essential for myeloid differentiation of the tumor cells and the resultant therapeutic outcome (Fig. 7I). These results are in line with previous work demonstrating that activation of the type I IFN pathway in leukemia cells has antiproliferative and proapoptotic effects, and promotes differentiation, resulting in abrogation of AML development (18, 52). Type I IFN therapy has previously been tested as a treatment option in AML, although these clinical trials have shown only limited success (53). One plausible explanation is the high toxicity and low stability of the IFN preparations used in those studies. To overcome this issue, more recent pegylated versions of recombinant type I IFN have been formulated, improving their tolerability and durability (54). In addition, a next generation of tumor-activating type I IFN with lower toxicity and prolonged half-life has recently been developed, masking IFN into a prodrug (ProIFN). In this design, IFN and IFNAR are genetically fused through a protease-cleavable linker that can be processed by matrix metallopeptidases, which are enriched in most tumors (55). As a result, IFN is activated locally inside the tumor. Yet, it is also possible that IFN has limited antileukemic effect as a single agent, and its clinical applicability will be improved in combination with other therapies, as our results suggest.

The use of HDACis as a single agent has resulted in moderate therapeutic efficacy in early-phase clinical trials of AML (12, 56). Recent studies combining HDACis with other anticancer agents have shown improved clinical outcomes (12, 53, 56). Specifically, combinations of HDACis with other anticancer drugs such as hypomethylating agents, all-trans retinoic acid, chemotherapy, or BET inhibitors are currently being tested in the clinic for patients with AML (53, 57), with panobinostat in combination with chemotherapeutic agents showing very promising results (58–60). Another option is to combine epigenetic drugs with immunotherapy, as mounting evidence shows that modulation of the immune system through epigenetic therapies can be leveraged to design better treatments for hematologic malignancies and many other types of cancer (23). In line with this, our results indicate that a regimen combining HDAC inhibition with type I IFN could significantly improve the efficacy of HDACis as anticancer treatments.

In summary, detailed single-cell molecular analysis using integrated genomics was used to discover a novel mechanism of epigenetic regulation of immune cells, specifically pDCs, that can be harnessed to improve the therapeutic effects of HDACis in several models of AML. Although we have focused on the role of pDCs, other immune cell types such as lymphocytes, macrophages, or granulocytes are likely to contribute to the beneficial effect of panobinostat. This requires further investigation. The results of our study highlight the importance of studying the effects of systemic therapies on both the host immune cells and tumor cells and demonstrate the complex molecular interplay between cells and signaling molecules within the tumor microenvironment. We harnessed this information to derive a new therapeutic regimen that was vastly superior to single-agent therapy. These results strongly suggest that combining HDAC inhibition with type I IFN would benefit patients with leukemia, including those with t(8;21) translocations.

METHODS

Experimental Mice and Materials

Wild-type C57BL/6 mice at 6 to 8 weeks of age were purchased from The Walter and Eliza Hall Institute of Medical Research. *Ifnar1*$^{-/-}$ null mice (20) were a generous gift from Paul Hertzog (Monash University). Animals were maintained under specific pathogen-free conditions and used in accordance with the institutional guidelines approved by the Peter MacCallum Cancer Centre Animal Ethics Committee (Approval numbers E472, E555, and E627). NSG (i.e., NOD.Cg-Prkdcscid Il2rgtm1Wjz/SzJ) and NRGS mice (i.e., NOD.Cg-Rag1tm1Mom Il2rgtm1Wjl Tg[CMV-IL3,CSF2,KITLG]1Eav/J) were imported from Jackson Laboratories. NSG mice were used to establish xenograft models with Kasumi-1 cells and cord blood; and NRGS mice were used for t(8;21);*NRAS*^{G13D} AML and *NRAS*^{mut} AML xenografts. All mice were kept pathogen-free in the animal facility of QIMR Berghofer Medical Research Institute and The Alfred Hospital. Mice received autoclaved and Baytril-treated (100 mg/L; Provet) water until 1 to 7 days before irradiation, and after that autoclaved and Septrin-treated water (12 mL/L cherry-flavored pediatric suspension, i.e., 96 mg/L trimethoprim, and 480 mg/L sulphamethoxazole; Arrow Pharmaceuticals). All mouse experiments were approved by the QIMR Berghofer ethics committee protocol A11605M and Alfred Medical Research and Education Precinct Animal Ethics Committee approval number: E/1940/2019/M.

Panobinostat (LBH589) was kindly provided by Novartis and prepared as a 2 mg/mL solution in 5% dextrose/dH_2O (D5W). Recombinant mouse interferon-alpha (rIFNα1) and IFNβ2 were kindly provided by Prof. Paul Hertzog (Monash University, Australia) and diluted in phosphate-buffered saline (PBS). Human IFNa2 was kindly provided by the Pharmacy Department of the Peter MacCallum Cancer Centre. Anti-PDCA1 (*InVivo*MAb anti-mouse CD317; cat. #BE0311) and IgG control (*InVivo*MAb anti-keyhole limpet hemocyanin; cat. #BE0090) were purchased from Bio X Cell. Poly(I:C) (HMW)/Lyovec was purchased from InvivoGen (tlrl-piclv). CpG 2216 (cat. #930507) was obtained from Tib Molbiol and complexed to DOTAP liposomal transfection reagent (Roche; cat. #11202375001)

for increased type I IFN induction. Poly I:C (cat. #27-4732-01) was purchased from GE Healthcare.

Xenograft Transplantation Experiments

Primary AML samples—collection of bone marrow aspirates—were obtained from patients with AML, after written informed consent in accordance with the Declaration of Helsinki, and approved by the QIMR Berghofer ethics committee protocol P1382 (HREC/14/QRBW/278) and The Alfred Hospital's human research ethics committees. Mononuclear cells were Ficoll-purified and red cell depleted. Viably frozen primary AML cells were thawed and CD3-depleted with biotinylated anti-human CD3 and biotin-binder Dynabeads (Invitrogen). Cells from $NRAS^{mut}$ patient sample RBWH-37 were subsequently injected via the lateral tail vein per 2.8 Gy sublethally irradiated (24 hours before transplant) NRGS recipient. For normal hematopoiesis studies (pDCs), viable mononuclear cells were isolated from cord blood samples by ficoll density gradient, CD3-depleted as above, and subsequently enriched for $CD34^+$ cells using the human CD34 MicroBead Kit (130-046-702 MACS Miltenyi Biotec) according to the manufacturer's instructions. Cells were injected via the lateral tail vein per sublethally irradiated NSG recipient. For CDXs, luciferase-expressing Kasumi-1 cells were expanded *in vitro* and transplanted per sublethally irradiated NSG recipient. Kasumi-1 cells tested negative for *Mycoplasma* during monthly testing, and their identity was confirmed by STR profiling.

Generation of A/E9a;$NRAS^{G12D}$–, M/E;$NRAS^{G12D}$–, or M/A;$NRAS^{G12D}$–Driven Leukemias

Retroviral transduction of mouse fetal liver cells (wild-type or *Ifnar1*$^{-/-}$) was performed as previously described (7). Briefly, viral producer cells (Phoenix) were transfected with MSCV-AML1/ETO9a-IRES-GFP+MSCV-Luc2-IRES-$NRAS^{G12D}$ vectors (A/E9a;$NRAS^{G12D}$); MSCV-MLL/ENL-IRES-GFP+MSCV-Luc2-IRES-$NRAS^{G12D}$ (M/E;$NRAS^{G12D}$) or MSCV-MLL/AF9-IRES-Luc2+MSCV-NRAS-IRES-mCherry (M/A;$NRAS^{G12D}$). Viral supernatants were mixed at a 1:1 ratio and used to transduce mouse fetal liver cells. To generate transplantable AML, 1×10^6 total cells per recipient were injected into lethally irradiated C57BL/6 mice (2×5.5 Gy; 4 hours apart; A/E9a;$NRAS^{G12D}$) or nonirradiated C57BL/6 mice (M/E;$NRAS^{G12D}$ and M/A;$NRAS^{G12D}$) via the tail vein. At least two different leukemic clones were used for secondary transplant experiments. To prevent infections, transplanted mice were provided with water containing neomycin and polymyxin B (both from Sigma).

Monitoring Leukemia

Tumor burden in transplanted mice was assessed by whole-body bioluminescence imaging (BLI) using an IVIS100 imaging system (PerkinElmer) and blood sampling. For BLI, mice were injected intraperitoneally (i.p.) with 50 mg/kg D-luciferin (PerkinElmer), anesthetized with isoflurane, and imaged for 2 minutes. Peripheral blood white cell counts were measured using an Advia 120 automated hematology analyzer (Bayer Diagnostics), and the percentage of GFP-positive cells was analyzed weekly by flow cytometry. Treatment started when the percentage of GFP-positive cells in the blood reached 10% to 20%. At the terminal disease stage, mice were euthanized, and leukemia cells were isolated from bone marrow (femur) and spleen. Single-cell suspensions were prepared, and cells were cryopreserved in fetal calf serum (FCS)/10% DMSO. To analyze differentiation of leukemia cells, May-Grünwald Giemsa (MGG) stain was performed on cytospins of FACS (GFP-positive) bone marrow cells. For PDX studies, leukemia was monitored through bone marrow aspiration on live mice. For Kasumi-1 CDX, mice were subcutaneously injected with 500 μg of D-luciferin (PerkinElmer), and 5 minutes after injection, luciferase signal intensity was analyzed using Xenogen IVIS 100 (Caliper Life Sciences).

In Vivo *Therapy*

Cryopreserved leukemia cells were thawed, washed, and resuspended in PBS. Approximately 1×10^6 cells per recipient were transplanted into sublethally irradiated mice (2×3 Gy; 4 hours apart) by tail-vein injection. Mice were monitored weekly, and treatment was initiated once leukemia was clearly established (corresponding to 10% to 20% GFP-positive cells in peripheral blood). For therapy studies, mice were treated daily with 25 mg/kg panobinostat, 5 consecutive days per week by i.p. injection for 1 week followed by 15 mg/kg panobinostat for 3 weeks. Control mice received the equivalent volume of vehicle. For combinatorial experiments, mice received 10,000U rIFNβ by i.p. injection, administered every other day for 4 weeks. Mortality events from advancing leukemia were recorded for the analysis of therapeutic efficacy. For short-term drug-response studies, mice received 25 mg/kg panobinostat, or equivalent volume of vehicle by i.p. injection once daily for indicated period prior to harvesting of spleen and bone marrow. Cell suspensions were prepared and used for further analyses. For pDC depletion experiments, mice were treated with 150 μg anti-PDCA1 or IgG control administered i.p. every other day. For xenotransplantation experiments, mice were treated with 10 mg/kg panobinostat and/or 10,000 U rIFNα2 on Monday, Wednesday, and Friday i.p. (or 3 μg/kg IFNα Pegasys once weekly subcutaneously) for 4 weeks.

Flow Cytometry

Cell suspensions were lysed in red cell lysis buffer (150 mmol/L NH_4Cl, 10 mmol/L $KHCO_3$, 0.1 mmol/L EDTA) and washed twice in FACS staining buffer (PBS supplemented with 2% FCS and 0.02% NaN_3). Aliquots of cells were preincubated with anti-CD16/CD32 (2.4G2) and stained on ice with anti-CD117 (c-Kit), anti-CD11b (Mac-1), anti-Ly6A/E (Sca1), anti-IFNAR1, anti-B220 (all from BD Biosciences), anti-CD11c, and anti–Siglec-H (both from BioLegend) in FACS staining buffer for at least 30 minutes. Tumor cells were identified using GFP reporter expression. For cell proliferation analysis, BrdU (100 μL of a 10 mg/mL stock; Sigma) was i.p. injected into mice 16 hours prior to euthanasia. Bone marrow cells were fixed, permeabilized, and stained using BrdU Flow Kit (BD Pharmingen), following the manufacturer's instructions. For dsRNA staining, cells were fixed and permeabilized (BD Pharmingen) and stained with K1-IgG2a monoclonal antibody (SCICONS; cat. #10020200) that recognizes dsRNA. To be detected by flow cytometry, K1-IgG2a was previously conjugated with APC using the APC conjugation kit from Innova Biosciences (cat. #705-0030). Human leukemia cells in PDXs were identified using anti-mouse CD45 (BD Biosciences) and the following anti-human antibodies: anti-CD45, anti-CD11b (both from BD Biosciences), anti-CD3, and anti-HLA-DR (both from BioLegend). We obtained written consent from the patients with AML to perform these experiments.

For live-dead cell discrimination, Sytox blue (Invitrogen) was used. All samples were pretreated for 10 minutes at room temperature with Human TruStain FcX Fc receptor blocking solution (BioLegend). For monitoring human AML cell engraftment, 25 to 50 μL of PB was stained after red blood cell lysis (BD Pharmlyse, BD Biosciences) with anti-human CD45 and anti-mouse CD45.1. For AML phenotyping, cell populations were purified from bone marrow (both femurs and tibiae) after red blood cell lysis and stained with anti-human CD45, anti-mouse CD45.1, anti-human CD34, and anti-mouse/human CD11b. For the analysis of normal hematopoiesis (pDCs), bone marrow cells were stained after red blood cell lysis with biotinylated lineage cocktail (anti-CD14, anti-CD3, anti-CD20, anti-CD66b, and anti-CD335), then washed and incubated in secondary antibody mix containing streptavidin, anti-human CD45-RA, anti-mouse/human CD11b, anti-human CD80, anti-human CD11c, anti-human CD86, anti-human CD45, anti-human HLA-DR, and anti-human CD123. Data were collected

on a FACSCanto II, LSR II, or LSRFortessa flow cytometer (BD Biosciences) and analyzed using FlowJo software (Tree Star).

Splenic Dendritic Cell Isolation

Spleens were collected into RPMI 1640 containing 2% FCS and dissociated with a scalpel and type 3 collagenase (Worthington) and DNase I, grade 2 (Roche), homogenizing for 20 minutes with a plastic Pasteur pipette. Then 0.1M EDTA was added, and the sample was homogenized for another 5 minutes. Single-cell suspensions were filtered through 40-μm cell strainers. Samples were enriched in DCs using OptiPrep (Axis-Shield; cat. #1114542) gradient, following the manufacturer's protocol for DC isolation from tissues. pDC and cDC populations were sorted in a BD FACSAria Fusion Cell Sorter (BD Bioscience) based on CD11c and Siglec-H expression, after exclusion of GFP$^+$ leukemia cells. For single-cell RNA-seq, spleens were enriched in DC using OptiPrep, and leukemia cells were removed through sorting, collecting GFP$^-$ cells. Then DCs were negatively selected using the EasySep Mouse Pan-DC Enrichment Kit (Stem Cell Technologies; cat. #19763).

Ex Vivo *Stimulation of Bone Marrow Cells*

Femur and tibia bones from IFNβ/YFP reporter mice (61) were isolated and kept in PBS. Bone marrow was flushed with RPMI 1640 medium without FCS using a 26G needle. Single cell suspensions were lysed using Erylysis-buffer (Morphisto) and filtered through 70-μm cell strainers. Cells were cultured in RPMI 1640 medium containing 1.6 nmol/L panobinostat or vehicle control (DMSO) for 24 hours before 1 μmol/L CpG 2216 or 0.1 μmol/L poly I:C was added to the culture for additional 12 or 24 hours. Percentage of IFNβ/YFP$^+$ cells of pDCs (gated as CD11c^{int} B220$^+$ CD11b$^-$) was determined by flow cytometry.

FLT3L-Derived Dendritic Cell Cultures

Bone marrow–derived FLT3L-cultured pDCs were generated as previously described (61). In short, single cell suspensions from mouse bone marrow were generated as described above. Cells were seeded at 20×10^6/10 cm petri dish (cell culture nontreated plates) in RPMI 1640 medium containing 100 ng/mL recombinant FLT3L (Bio X Cell). At day 5, cells were collected and fresh media were added. pDCs were sorted at day 7 (gated as CD11c$^+$Siglec-H$^+$) and incubated with vehicle, panobinostat, or poly I:C for 6 hours.

Immunoblot

Protein lysates were prepared using cell lysis buffer (150 mmol/L NaCl, 10 mmol/L Tris-HCl [pH 7.4], 5 mmol/L EDTA, 1% Triton X-100) supplemented with PMSF and the cOmplete protease inhibitor cocktail (EDTA-free; Roche). Lysates were subjected to SDS-PAGE and transferred to PVDF membrane (Millipore). Membranes were blocked in skimmed milk or BSA and probed overnight with the following antibodies: anti-AML1 (Cell Signaling Technology; cat. #4336); anti-acetyl-histone H3 (Millipore; cat. #06-599); anti-histone H3 (Abcam; cat. #1791); and anti-α-actin (Sigma; cat. #AC-74). Filters were then washed, and probed with either anti-mouse horseradish peroxidase (HRP) or anti-rabbit HRP (both DakoCytomation) secondary antibodies. Signals were visualized using enhanced chemiluminescent detection reagent (Amersham).

Quantitative RT-PCR

Total RNA from FACS tumor cells (GFP$^+$) was isolated using TRIzol (Invitrogen) following the manufacturer's protocol. Synthesis of cDNA was performed following standard protocols using MMLV Reverse Transcriptase (Promega). Quantitative RT-PCR was performed using SYBR Green (Applied Biosystems) method in a 384-well format using the ABI Prism 7900HT (Applied Biosystems) or a 96-well format StepOne Plus (Applied Biosystems). For quantification, the C_T values were obtained and normalized to the C_T values of *Hprt* or *Actin* gene. Fold changes in expression were calculated by the $2^{-\Delta\Delta CT}$ method. To detect the AML1–ETO fusion transcript, total RNA was extracted from cells isolated from the bone marrow of transplanted mice using TRIzol (Invitrogen), following manufacturer's protocol. Synthesis of cDNA was performed using LunaScript RT Supermix (NEB). PCR was performed using KAPA Taq polymerase (Roche) in an Eppendorf Master cycler. PCR products were separated on a 2% agarose gel using standard protocols. Primer sets used for gene-expression analysis and for the AML1–ETO transcript can be found in Supplementary Table S10.

Microarray, RNA-seq, and Analysis

Following 3 days of treatment with panobinostat or vehicle, tumor cells (GFP$^+$) were sorted on a BD FACSAriaII cell sorter (BD Biosciences), and propidium iodide was used as a viability marker. Total RNA was prepared from three independent replicates using TRIzol (Invitrogen) following the manufacturer's protocol. Samples were further purified using the RNeasy MinElute Kit (Qiagen) or Direct-zol RNA Miniprep Kit (Zymo Research). mRNA libraries for A/E9a;NRAS^{G12D} tumor cells were generated using TruSeq RNA Library Prep Kit (Illumina) and sequenced in a HiSeq2000 sequencer SE50bp (Illumina). Microarray for A/E9a;NRAS^{G12D} tumor cells was performed using Affymetrix MoGene-1_0-st-v1. Data were analyzed using Limma in R. mRNA libraries for A/E9a;NRAS^{G12D};*Ifnar1*$^{-/-}$ tumor cells were generated using the TruSeq RNA Library Prep Kit (Illumina) and sequenced in a HiSeq2500 sequencer PE50bp (Illumina). mRNA libraries for DCs, sorted from the spleens of A/E9a; NRAS^{G12D} leukemia–bearing mice after 2 days of treatment with panobinostat or vehicle, were generated using NEB Next Single-Cell/Low Input RNA Library Preparation Kit (New England Biolabs) and sequenced in a NextSeq500 sequencer SE75bp (Illumina). Sequencing files were demultiplexed (Bcl2fastq, v2.17.1.14), and quality control (QC) was performed on FASTQ files using FASTQC (v0.11.6). Sequencing reads were trimmed (cutadapt v2.1) and aligned to the mm10 mouse reference genome using HISAT2 (v2.1.0). Read counting across genomic features was performed using FeatureCounts (Subread, v2.0.0), and differential gene-expression analysis was performed using Voom-Limma in R (v3.42.2). GSEAs were performed using the Broad Institute GSEA software (62).

ChIP-seq

Twenty thousand DCs, sorted from the spleens of A/E9a;NRAS^{G12D} leukemia–bearing mice after 2 days of treatment with panobinostat or vehicle, were fixed with 1% formaldehyde for 6 minutes and sonicated using the S220 Focused-ultrasonicator (Covaris) for 8 minutes. Samples were incubated with an antibody to H3K27Ac (Abcam; cat. #ab4729), and chromatin was isolated with the True Microchip Kit (Diagenode; cat. #C01010130) according to the manufacturer's instructions. Libraries were prepared using the DNA Library Prep NEB (New England Biolabs) and sequenced in a NextSeq500 sequencer SE75bp (Illumina).

Bcl2fastq (v2.17.1.14) was used to demultiplex sequencing files, and resulting Fastq output was quality checked using FASTQC (v0.11.6). Fastq read alignment to the mouse genome (mm10/GRCm38) was performed using Botwtie2 (v2.3.4.1). SAM files generated were converted to BAM file format and subsequently sorted, indexed, and potential PCR duplicates were removed using Samtools (v1.9) with view, sort, index, and rmdup functions, respectively. Deeptools (v3.0.0) bamCoverage function was used for BAM to BigWig file conversion using the following settings (–normalizeUsing CPM–smooth length 150 -bs 50 -e 225).

BigWig file average read density across defined genomic intervals was performed using Deeptools (v3.0.0) computeMatrix function

with the following settings (reference-point –referencePoint center –upstream 2000 –downstream 2000 -bs 50 –missingDataAsZero), where average read density was calculated ±2 Kb of ATAC peak summits and genomic regions spanning mm10 blacklist intervals (ENCODE, accession ENCFF547MET) were removed. Resulting matrices were subsequently used to generate heatmap and average profile plots with Deeptools (v3.0.0) plotHeatmap and Rstudio (v3.6.1), respectively.

BAM file peak calling was performed MACS (v2.1.1) with the following settings (-f BAM -m 10 30 –broad –cutoff-analysis -g mm -c INPUT), and resulting BED files were filtered for regions spanning mm10 blacklist intervals (ENCODE, accession ENCFF547MET) and modified into GFF file format using Rstudio (v3.6.1) to meet input criteria for ROSE2 (v1.0.5).

ATAC-seq

Fifteen thousand DCs, sorted from the spleens of A/E9a;NRAS^{G12D} leukemia–bearing mice after 2 days of treatment with panobinostat or vehicle, were lysed in cold ATAC-seq cell lysis buffer and exposed to Tn5 transposase (Nextera) for 30 minutes at 37°C. Transposed chromatin was amplified using customized Nextera PCR Primer 1 and Primer 2 (barcode; ref. 36) and HotStart KAPA ReadyMix (Roche). Libraries were quantified by Qubit using the DS DNA HS Kit (Thermo Fisher Scientific), QC validated using the Tape Station DNA High-Sensitivity D1K (Agilent), size-selected using Pippen Prep 1.5% Agarose Gel cassettes (Sage Science) and sequenced in a NextSeq500 sequencer SE75bp (Illumina).

Similar to ChIP-seq analysis, Bcl2fastq (v2.17.1.14) was used to demultiplex sequencing files and resulting Fastq output was quality checked using FASTQC (v0.11.6). Fastq read alignment to the mouse genome (mm10/GRCm38) was performed using Botwtie2 (v2.3.4.1). SAM files generated were converted to BAM file format and subsequently sorted, indexed, and potential PCR duplicates were removed using Samtools (v1.9) with view, sort, index and rmdup functions, respectively. Deeptools (v3.0.0) bamCoverage function was used for BAM to BigWig file conversion using the following settings (–normalizeUsing CPM –smooth length 150 -bs 50 -e 225).

BAM file peak calling was performed MACS (v2.1.1) with the following settings (-g mm -f BAM –call-summits –nomodel –extsize 100). BigWig file average read density across defined genomic intervals was performed using Deeptools (v3.0.0) computeMatrix function with the following settings (reference-point –referencePoint center –upstream 2000 –downstream 2000 -bs 50) where average read density was calculated ±2 Kb of ATAC peak summits.

Single Cell Sequencing Methods: Ab-Staining, Capture of Cells in GEMs, Barcoding of Transcriptomes, and Library Preparation

DCs—isolated from spleens through OptiPrep gradient, followed by sorting of GFP$^-$ cells and magnetic negative selection—were incubated with Cell Hashing HTO-conjugated antibodies (BioLegend, TotalSeq anti-mouse Hashtag reagents; cat. #A0301-A0306) and CITE-seq antibodies (BioLegend, TotalSeq-A0106 anti-mouse CD11c and A0119 anti-mouse Siglec-H), as described previously (27, 28). Cells were washed 3 times with FACS buffer, and samples were pooled at an equal concentration of 1,500 cells/μL. Pooled DC samples were loaded onto the 10X Chromium instrument (10X Genomics) to generate single-cell Gel Beads-in-Emulsion (GEM) and capture/barcode cells. All samples followed the 10X Genomics Single-Cell 3′ v3 according to the manufacturer's instructions up until the cDNA amplification step (10X Genomics). Two picomoles of HTO and ADT additive oligonucleotides were spiked into the cDNA amplification PCR, and cDNA was amplified according to the 10X Single-Cell 3′ v3 protocol (10X Genomics). Following cDNA amplification, 0.6× SPRI was used to separate the large cDNA fraction derived from cellular mRNAs (retained on beads) from the ADT- and Cell Hashtag (HTO)–containing fraction (in supernatant). The cDNA fraction was processed according to the 10X Genomics Single Cell 3′ v3 protocol to generate the transcriptome library; indexing was done using Chromium i7 Multiplex Kit. An additional 1.4X reaction volume of SPRI beads was added to the ADT/HTO fraction to bring the ratio up to 2.0X. The beads were washed with 80% ethanol, eluted in water, and an additional round of 2.0X SPRI was performed to remove excess single-stranded oligonucleotides from cDNA amplification. After final elution, separate PCRs were set up to generate the CITE-seq ADT library (SI-PCR and RPI-x primers) and the HTO library (SI-PCR and D7xx_s).

Single Cell RNA-seq Analysis

10X Genomics' Cell Ranger Software (v3.1.0) was used to align reads to the mm10/GRCm38 reference genome, demultiplex cellular barcodes and quantify unique molecular identifiers and antibody capture (HTOs and ADTs). Intersample doublets and intrasample doublets were removed using Seurat's HTODemux function and the Scrublet python package (v0.2.1; ref. 63), respectively. In more detail, counts with more than one median absolute derivation above the median Scrublet score were retained.

The SCENIC method (33) was used to estimate relative transcription factor activity in each cell. Calculation of AUC scores for TFs was performed using inferred using gene regulatory networks with the pyscenic python package (v3.6.1).

The Seurat R package (v3.1.0; ref. 64) was used to process gene expression and antibody count matrices within R studio (v3.6.1). Seurat's SCTransform function was subsequently used to sctransform normalize RNA transcript counts for barcodes identified as cells by Cell Ranger. Transformation of counts with no covariates in the sctranform model was first performed, then Seurat's CellCycleScoring function with cell-cycle gene sets of mouse homologs was used to calculate cell-cycle phase scores. Cell-cycle phase scores and the percentage of raw RNA counts belonging to mitochondrial genes for each cell were used to rerun sctransform normalization and regress out of the model.

Centered log ratio transformation was performed to normalize ADT counts.

Sctransform-scaled RNA expression values for genes with residual variance greater than 1.3 in the sctransform model were used for PCA. The top 10 principal components were used to calculate a shared nearest-neighbors (SNN) network with the FingNeighbors function with a cosine distance metric and 50 k-nearest neighbors. Cell populations were subsequently identified using the SNN network and the FindClusters function with the Louvain algorithm and a resolution parameter of 0.6. The top 10 principal components were also used to calculate UMAP values using the RunUMAP function with a cosine distance metric and 50 nearest neighbors as parameters.

Analysis of Core Regulatory Circuitries

Putative SE regions from H3K27Ac ChIP-seq peaks were identified using the Ranking Ordering of Super-Enhancer (ROSE2; v1.0.5) algorithm (65, 66) with the following settings (-g MM10 -c INPUT -s 12500 -t 2000), where enhancer peaks within 12.5 Kb were stitched, and peaks within 2 Kb of a TSS were excluded to remove promoter bias.

The Coltron (v1.0.2) algorithm was used to construct transcription factor regulatory networks using H3K27Ac ChIP-seq signal (BAM file) and ROSE2 generated enhancer table to identify SE-associated TFs, and ATAC narrowPeak BED file to search for TF motifs within SE regions. Remaining parameters were left as default. Clique fractions were calculated as the number of cliques a TF participates in divided by the number to total cliques.

Data Availability

All sequencing data sets are available on the Gene Expression Omnibus under accession number GSE198119.

Authors' Disclosures

F. Rossello reports grants from the National Health and Medical Research Council (Australia), and other support from The Lorenzo and Pamela Galli Medical Research Trust and The PMF Foundation during the conduct of the study. S. Bjelosevic reports grants from Cancer Council Victoria during the conduct of the study. J. Lichte reports grants from the German Research Foundation (DFG) during the conduct of the study. S.J. Hogg reports grants from Cancer Council Victoria and the National Health and Medical Research Council of Australia during the conduct of the study. L.M. Kats reports grants and personal fees from Agios Pharmaceuticals, and grants from Servier Pharmaceuticals and Biocurate outside the submitted work. D.D. De Carvalho reports other support from Adela and grants from Pfizer outside the submitted work. S. Scheu reports grants from the German Research Foundation (DFG) during the conduct of the study, as well as a patent for bicistronic mRNA licensed and with royalties paid. S.W. Lane reports personal fees from Novartis, AbbVie, and Astellas, and grants from Celgene/Bristol Myers Squibb outside the submitted work. A.H. Wei reports nonfinancial support from Helsinn and grants, personal fees, and nonfinancial support from Novartis during the conduct of the study; grants, personal fees, and nonfinancial support from AbbVie and Bristol Myers Squibb, and grants and personal fees from Servier, Pfizer, AstraZeneca, Janssen, and Amgen outside the submitted work; and is an employee of the Walter and Eliza Hall Institute of Medical Research and eligible for royalty payments in relation to venetoclax. R.W. Johnstone reports grants, personal fees, and nonfinancial support from Novartis during the conduct of the study, as well as grants from Roche, Bristol Myers Squibb, and AstraZeneca, and grants and personal fees from MycRx outside the submitted work. No disclosures were reported by the other authors.

Authors' Contributions

J.M. Salmon: Conceptualization, resources, data curation, formal analysis, supervision, investigation, methodology, writing–original draft, writing–review and editing. **I. Todorovski:** Formal analysis, investigation, methodology. **K.L. Stanley:** Investigation. **C. Bruedigam:** Resources, investigation, visualization. **C.J. Kearney:** Formal analysis, investigation. **L.G. Martelotto:** Resources, investigation. **F. Rossello:** Resources, data curation. **T. Semple:** Resources, investigation, methodology. **G. Mir Arnau:** Resources, investigation, methodology. **M. Zethoven:** Data curation, formal analysis. **M. Bots:** Conceptualization, resources. **S. Bjelosevic:** Formal analysis, investigation. **L.A. Cluse:** Validation, investigation. **P.J. Fraser:** Formal analysis, investigation. **V. Litalien:** Resources, investigation. **E. Vidacs:** Validation, investigation. **K. McArthur:** Investigation. **A.Y. Matthews:** Resources, investigation. **E. Gressier:** Resources, investigation. **N.A. de Weerd:** Resources, investigation. **J. Lichte:** Resources, investigation. **M.J. Kelly:** Data curation, formal analysis, investigation. **S.J. Hogg:** Data curation, formal analysis, validation, investigation. **P.J. Hertzog:** Resources, supervision. **L.M. Kats:** Conceptualization, resources, investigation. **S.J. Vervoort:** Conceptualization, formal analysis, supervision. **D.D. De Carvalho:** Resources, visualization. **S. Scheu:** Resources, methodology. **S. Bedoui:** Resources, investigation. **B.T. Kile:** Conceptualization, resources, supervision. **S.W. Lane:** Conceptualization, resources, investigation. **A.C. Perkins:** Resources, supervision. **A.H. Wei:** Resources, investigation. **P.M. Dominguez:** Conceptualization, resources, data curation, formal analysis, supervision, funding acquisition, investigation, visualization, methodology, writing–original draft, project administration, writing–review and editing. **R.W. Johnstone:** Conceptualization, resources, formal analysis, supervision, funding acquisition, investigation, visualization, writing–original draft, project administration, writing–review and editing.

Acknowledgments

We thank staff from the Animal Facility, Genotyping Core, Flow Cytometry Facility, Molecular Genomics Core, Victorian Center for Functional Genomics, Centre for Advanced Histology and Microscopy and Bioinformatics Consulting Core of the Peter MacCallum Cancer Centre, and members of the Johnstone laboratory for useful discussions. We acknowledge Nicole Messina and Dan Andrews for providing reagents and advice and support from the Peter MacCallum Cancer Centre Foundation and Australian Cancer Research Foundation. We also thank the Monash Histology Platform and Gareth Gregory for processing and assessing, respectively, the histology sections from the PDX models. Research reported in this publication was supported by Cure Cancer Australia under award number 1051444, awarded to J.M. Salmon and R.W. Johnstone. I. Todorovski was supported by an Australian Research Training Program (RTP) Scholarship during this study; S.J. Vervoort was supported by a Rubicon Fellowship from the Netherlands Organization for Scientific Research (NWO; 019.161LW.017), a National Health and Medical Research Council (NHMRC) EL1 Fellowship (GNT1178339), and a Peter MacCallum Cancer Foundation Grant; S.J. Hogg was supported by a Postdoctoral Fellowship from Cancer Council Victoria (CCV); L.G. Martelotto and Single Cell Innovation Lab were supported by The Lorenzo and Pamela Galli Research Fund Trust; L.M. Kats was supported by a Victorian Cancer Agency Fellowship (MCRF15003); S. Scheu was supported by the German Research Foundation (DFG; 270650915/GRK2158 and SCHE692/6-1) and the Manchot Graduate School "Molecules of Infection III"; D.D. De Carvalho is funded by the Canadian Institute of Health Research (201512MSH360794-228629, FDN 148430, and PJT 165986) and the Canada Research Chairs; B.T. Kile is funded by a Project Grant from NHMRC (Grant No. 1113577) and an NHMRC Principal Research Fellowship (No. 1063008); P.M. Dominguez was supported by a Postdoctoral Fellowship Grant from the Lymphoma Research Foundation and is funded by an Ideas Grant from the NHMRC (GNT2011217); and R.W. Johnstone is funded by a Project Grant from CCV, a Project Grant and Program Grant (grant 454569) from the NHMRC, an NHMRC Senior Principal Research Fellowship, and a Grant from The Kids' Cancer Project (to R.W. Johnstone and S.J. Vervoort).

The costs of publication of this article were defrayed in part by the payment of page charges. This article must therefore be hereby marked *advertisement* in accordance with 18 U.S.C. Section 1734 solely to indicate this fact.

Received August 10, 2020; revised October 28, 2021; accepted March 16, 2022; published first March 21, 2022.

REFERENCES

1. Ustun C, Marcucci G. Emerging diagnostic and therapeutic approaches in core binding factor acute myeloid leukaemia. Curr Opin Hematol 2015;22:85–91.
2. Solh M, Yohe S, Weisdorf D, Ustun C. Core-binding factor acute myeloid leukemia: heterogeneity, monitoring, and therapy. Am J Hematol 2014;89:1121–31.
3. Frank R, Zhang J, Uchida H, Meyers S, Hiebert SW, Nimer SD. The AML1/ETO fusion protein blocks transactivation of the GM-CSF promoter by AML1B. Oncogene 1995;11:2667–74.
4. Liu Y, Chen W, Gaudet J, Cheney MD, Roudaia L, Cierpicki T, et al. Structural basis for recognition of SMRT/N-CoR by the MYND domain and its contribution to AML1/ETO's activity. Cancer Cell 2007;11:483–97.

5. Cancer Genome Atlas Research N, Ley TJ, Miller C, Ding L, Raphael BJ, Mungall AJ, et al. Genomic and epigenomic landscapes of adult de novo acute myeloid leukemia. N Engl J Med 2013;368:2059–74.
6. Zuber J, Radtke I, Pardee TS, Zhao Z, Rappaport AR, Luo W, et al. Mouse models of human AML accurately predict chemotherapy response. Genes Dev 2009;23:877–89.
7. Bots M, Verbrugge I, Martin BP, Salmon JM, Ghisi M, Baker A, et al. Differentiation therapy for the treatment of t(8;21) acute myeloid leukemia using histone deacetylase inhibitors. Blood 2014;123:1341–52.
8. Sun XJ, Wang Z, Wang L, Jiang Y, Kost N, Soong TD, et al. A stable transcription factor complex nucleated by oligomeric AML1–ETO controls leukaemogenesis. Nature 2013;500:93–7.
9. Wang J, Hoshino T, Redner RL, Kajigaya S, Liu JM. ETO, fusion partner in t(8;21) acute myeloid leukemia, represses transcription by interaction with the human N-CoR/mSin3/HDAC1 complex. Proc Natl Acad Sci U S A 1998;95:10860–5.
10. Lillico R, Lawrence CK, Lakowski TM. Selective DOT1L, LSD1, and HDAC class I inhibitors reduce HOXA9 expression in MLL-AF9 rearranged leukemia cells, but dysregulate the expression of many histone-modifying enzymes. J Proteome Res 2018;17:2657–67.
11. Ye J, Zha J, Shi Y, Li Y, Yuan D, Chen Q, et al. Co-inhibition of HDAC and MLL-menin interaction targets MLL-rearranged acute myeloid leukemia cells via disruption of DNA damage checkpoint and DNA repair. Clin Epigenetics 2019;11:137.
12. Suraweera A, O'Byrne KJ, Richard DJ. Combination therapy with histone deacetylase inhibitors (HDACi) for the treatment of cancer: achieving the full therapeutic potential of HDACi. Front Oncol 2018;8:92.
13. West AC, Smyth MJ, Johnstone RW. The anticancer effects of HDAC inhibitors require the immune system. Oncoimmunology 2014;3:e27414.
14. Fennell KA, Bell CC, Dawson MA. Epigenetic therapies in acute myeloid leukemia: where to from here? Blood 2019;134:1891–901.
15. Falkenberg KJ, Johnstone RW. Histone deacetylases and their inhibitors in cancer, neurological diseases and immune disorders. Nat Rev Drug Discov 2014;13:673–91.
16. Conte M, De Palma R, Altucci L. HDAC inhibitors as epigenetic regulators for cancer immunotherapy. Int J Biochem Cell Biol 2018;98:65–74.
17. Salmon JM, Bots M, Vidacs E, Stanley KL, Atadja P, Zuber J, et al. Combining the differentiating effect of panobinostat with the apoptotic effect of arsenic trioxide leads to significant survival benefit in a model of t(8;21) acute myeloid leukemia. Clin Epigenetics 2015;7:2.
18. Anguille S, Lion E, Willemen Y, Van Tendeloo VF, Berneman ZN, Smits EL. Interferon-alpha in acute myeloid leukemia: an old drug revisited. Leukemia 2011;25:739–48.
19. Budhwani M, Mazzieri R, Dolcetti R. Plasticity of type I interferon-mediated responses in cancer therapy: from anti-tumor immunity to resistance. Front Oncol 2018;8:322.
20. Hwang SY, Hertzog PJ, Holland KA, Sumarsono SH, Tymms MJ, Hamilton JA, et al. A null mutation in the gene encoding a type I interferon receptor component eliminates antiproliferative and antiviral responses to interferons alpha and beta and alters macrophage responses. Proc Natl Acad Sci U S A 1995;92:11284–8.
21. Chiappinelli KB, Strissel PL, Desrichard A, Li H, Henke C, Akman B, et al. Inhibiting DNA methylation causes an interferon response in cancer via dsRNA including endogenous retroviruses. Cell 2015;162:974–86.
22. Roulois D, Loo Yau H, Singhania R, Wang Y, Danesh A, Shen SY, et al. DNA-demethylating agents target colorectal cancer cells by inducing viral mimicry by endogenous transcripts. Cell 2015;162:961–73.
23. Jones PA, Ohtani H, Chakravarthy A, De Carvalho DD. Epigenetic therapy in immune-oncology. Nat Rev Cancer 2019;19:151–61.
24. Ali S, Mann-Nuttel R, Schulze A, Richter L, Alferink J, Scheu S. Sources of type I interferons in infectious immunity: plasmacytoid dendritic cells not always in the driver's seat. Front Immunol 2019;10:778.
25. Reizis B. Plasmacytoid dendritic cells: development, regulation, and function. Immunity 2019;50:37–50.
26. Guilliams M, Ginhoux F, Jakubzick C, Naik SH, Onai N, Schraml BU, et al. Dendritic cells, monocytes and macrophages: a unified nomenclature based on ontogeny. Nat Rev Immunol 2014;14:571–8.
27. Stoeckius M, Hafemeister C, Stephenson W, Houck-Loomis B, Chattopadhyay PK, Swerdlow H, et al. Simultaneous epitope and transcriptome measurement in single cells. Nat Methods 2017;14:865–8.
28. Stoeckius M, Zheng S, Houck-Loomis B, Hao S, Yeung BZ, Mauck WM 3rd, et al. Cell Hashing with barcoded antibodies enables multiplexing and doublet detection for single cell genomics. Genome Biol 2018;19:224.
29. Brown CC, Gudjonson H, Pritykin Y, Deep D, Lavallee VP, Mendoza A, et al. Transcriptional basis of mouse and human dendritic cell heterogeneity. Cell 2019;179:846–63.
30. Maier B, Leader AM, Chen ST, Tung N, Chang C, LeBerichel J, et al. A conserved dendritic-cell regulatory program limits antitumour immunity. Nature 2020;580:257–62.
31. Di Pilato M, Kfuri-Rubens R, Pruessmann JN, Ozga AJ, Messemaker M, Cadilha BL, et al. CXCR6 positions cytotoxic T cells to receive critical survival signals in the tumor microenvironment. Cell 2021;184:4512–30.
32. Becht E, McInnes L, Healy J, Dutertre C-A, Kwok IWH, Ng LG, et al. Dimensionality reduction for visualizing single-cell data using UMAP. Nat Biotechnol 2019;37:38–44.
33. Aibar S, Gonzalez-Blas CB, Moerman T, Huynh-Thu VA, Imrichova H, Hulselmans G, et al. SCENIC: single-cell regulatory network inference and clustering. Nat Methods 2017;14:1083–6.
34. Swiecki M, Wang Y, Vermi W, Gilfillan S, Schreiber RD, Colonna M. Type I interferon negatively controls plasmacytoid dendritic cell numbers in vivo. J Exp Med 2011;208:2367–74.
35. Shestakova E, Bandu MT, Doly J, Bonnefoy E. Inhibition of histone deacetylation induces constitutive derepression of the beta interferon promoter and confers antiviral activity. J Virol 2001;75:3444–52.
36. Buenrostro JD, Giresi PG, Zaba LC, Chang HY, Greenleaf WJ. Transposition of native chromatin for fast and sensitive epigenomic profiling of open chromatin, DNA-binding proteins and nucleosome position. Nat Methods 2013;10:1213–8.
37. Lin CY, Erkek S, Tong Y, Yin L, Federation AJ, Zapatka M, et al. Active medulloblastoma enhancers reveal subgroup-specific cellular origins. Nature 2016;530:57–62.
38. Ott CJ, Federation AJ, Schwartz LS, Kasar S, Klitgaard JL, Lenci R, et al. Enhancer architecture and essential core regulatory circuitry of chronic lymphocytic leukemia. Cancer Cell 2018;34:982–95.
39. Saint-Andre V, Federation AJ, Lin CY, Abraham BJ, Reddy J, Lee TI, et al. Models of human core transcriptional regulatory circuitries. Genome Res 2016;26:385–96.
40. Cisse B, Caton ML, Lehner M, Maeda T, Scheu S, Locksley R, et al. Transcription factor E2-2 is an essential and specific regulator of plasmacytoid dendritic cell development. Cell 2008;135:37–48.
41. Birmachu W, Gleason RM, Bulbulian BJ, Riter CL, Vasilakos JP, Lipson KE, et al. Transcriptional networks in plasmacytoid dendritic cells stimulated with synthetic TLR 7 agonists. BMC Immunol 2007;8:26.
42. Sichien D, Scott CL, Martens L, Vanderkerken M, Van Gassen S, Plantinga M, et al. IRF8 transcription factor controls survival and function of terminally differentiated conventional and plasmacytoid dendritic cells, respectively. Immunity 2016;45:626–40.
43. Honda K, Yanai H, Negishi H, Asagiri M, Sato M, Mizutani T, et al. IRF-7 is the master regulator of type-I interferon-dependent immune responses. Nature 2005;434:772–7.
44. Pfeffer LM. The role of nuclear factor kappaB in the interferon response. J Interferon Cytokine Res 2011;31:553–9.
45. Dress RJ, Dutertre CA, Giladi A, Schlitzer A, Low I, Shadan NB, et al. Plasmacytoid dendritic cells develop from Ly6D(+) lymphoid progenitors distinct from the myeloid lineage. Nat Immunol 2019;20:852–64.
46. Gambacorta V, Gnani D, Vago L, Di Micco R. Epigenetic therapies for acute myeloid leukemia and their immune-related effects. Front Cell Dev Biol 2019;7:207.
47. Aspeslagh S, Morel D, Soria JC, Postel-Vinay S. Epigenetic modifiers as new immunomodulatory therapies in solid tumours. Ann Oncol 2018;29:812–24.

48. Bornstein C, Winter D, Barnett-Itzhaki Z, David E, Kadri S, Garber M, et al. A negative feedback loop of transcription factors specifies alternative dendritic cell chromatin States. Mol Cell 2014;56:749–62.
49. Liu S, Klisovic RB, Vukosavljevic T, Yu J, Paschka P, Huynh L, et al. Targeting AML1/ETO-histone deacetylase repressor complex: a novel mechanism for valproic acid-mediated gene expression and cellular differentiation in AML1/ETO-positive acute myeloid leukemia cells. J Pharmacol Exp Ther 2007;321:953–60.
50. Amann JM, Nip J, Strom DK, Lutterbach B, Harada H, Lenny N, et al. ETO, a target of t(8;21) in acute leukemia, makes distinct contacts with multiple histone deacetylases and binds mSin3A through its oligomerization domain. Mol Cell Biol 2001;21:6470–83.
51. Barbetti V, Gozzini A, Rovida E, Morandi A, Spinelli E, Fossati G, et al. Selective anti-leukaemic activity of low-dose histone deacetylase inhibitor ITF2357 on AML1/ETO-positive cells. Oncogene 2008;27:1767–78.
52. DeKelver RC, Lewin B, Weng S, Yan M, Biggs J, Zhang DE. RUNX1-ETO induces a type I interferon response which negatively effects t(8;21)-induced increased self-renewal and leukemia development. Leuk Lymphoma 2014;55:884–91.
53. San Jose-Eneriz E, Gimenez-Camino N, Agirre X, Prosper F. HDAC inhibitors in acute myeloid leukemia. Cancers 2019;11:1794.
54. Cuartero S, Innes AJ, Merkenschlager M. Towards a better understanding of cohesin mutations in AML. Front Oncol 2019;9:867.
55. Cao X, Liang Y, Hu Z, Li H, Yang J, Hsu EJ, et al. Next generation of tumor-activating type I IFN enhances anti-tumor immune responses to overcome therapy resistance. Nat Commun 2021;12:5866.
56. Saygin C, Carraway HE. Emerging therapies for acute myeloid leukemia. J Hematol Oncol 2017;10:93.
57. Klisovic MI, Maghraby EA, Parthun MR, Guimond M, Sklenar AR, Whitman SP, et al. Depsipeptide (FR 901228) promotes histone acetylation, gene transcription, apoptosis and its activity is enhanced by DNA methyltransferase inhibitors in AML1/ETO-positive leukemic cells. Leukemia 2003;17:350–8.
58. Ocio EM, Herrera P, Olave MT, Castro N, Perez-Simon JA, Brunet S, et al. Panobinostat as part of induction and maintenance for elderly patients with newly diagnosed acute myeloid leukemia: phase Ib/II panobidara study. Haematologica 2015;100:1294–300.
59. Bug G, Burchert A, Wagner EM, Kroger N, Berg T, Guller S, et al. Phase I/II study of the deacetylase inhibitor panobinostat after allogeneic stem cell transplantation in patients with high-risk MDS or AML (PANOBEST trial). Leukemia 2017;31:2523–5.
60. DeAngelo DJ, Walker AR, Schlenk RF, Sierra J, Medeiros BC, Ocio EM, et al. Safety and efficacy of oral panobinostat plus chemotherapy in patients aged 65 years or younger with high-risk acute myeloid leukemia. Leuk Res 2019;85:106197.
61. Scheu S, Dresing P, Locksley RM. Visualization of IFNbeta production by plasmacytoid versus conventional dendritic cells under specific stimulation conditions in vivo. Proc Natl Acad Sci U S A 2008;105:20416–21.
62. Subramanian A, Tamayo P, Mootha VK, Mukherjee S, Ebert BL, Gillette MA, et al. Gene set enrichment analysis: a knowledge-based approach for interpreting genome-wide expression profiles. Proc Natl Acad Sci U S A 2005;102:15545–50.
63. Wolock SL, Lopez R, Klein AM. Scrublet: computational identification of cell doublets in single-cell transcriptomic data. Cell Syst 2019;8:281–91.
64. Stuart T, Butler A, Hoffman P, Hafemeister C, Papalexi E, Mauck WM 3rd, et al. Comprehensive integration of single-cell data. Cell 2019;177:1888–902.
65. Whyte WA, Orlando DA, Hnisz D, Abraham BJ, Lin CY, Kagey MH, et al. Master transcription factors and mediator establish super-enhancers at key cell identity genes. Cell 2013;153:307–19.
66. Loven J, Hoke HA, Lin CY, Lau A, Orlando DA, Vakoc CR, et al. Selective inhibition of tumor oncogenes by disruption of super-enhancers. Cell 2013;153:320–34.